STOCHASTIC AND KINETIC COALESCENCE MODELS FOR RAIN FORMATION IN WARM CLOUDS

by

Vasylyna Bohun
Specialist with distinction Poltava State Pedagogical University 2000
M.Sc. with distinction Poltava State Pedagogical University 2002

A Thesis Submitted in Partial Fullfillment of the
Requirements for the Degree of
MASTER OF SCIENCE
in the Department of Mathematics and Statistics

Supervisory Committee

Stochastic and Kinetic Coalescence Models for Rain Formation in Warm Clouds

by

Vasylyna Bohun

University of Victoria

Dr. Reinhard Illner, (Department of Mathematics and Statistics)
Co-Supervisor

Dr. Boualem Khouider, (Department of Mathematics and Statistics)
Co-Supervisor

Dr. Martial Agueh, (Department of Mathematics and Statistics)
Departament Member

Dr. Knut von Salzen, (School of Earth and Ocean Sciences and Canadian Centre for Climate Modelling and Analysis)
Outside Member

Table of Contents

Supervisory Committee

Dr. Reinhard Illner, (Department of Mathematics and Statistics)
Co-Supervisor

Dr. Boualem Khouider, (Department of Mathematics and Statistics)
Co-Supervisor

Dr. Martial Agueh, (Department of Mathematics and Statistics)
Departament Member

Dr. Knut von Salzen, (School of Earth and Ocean Sciences and Canadian Centre for Climate Modelling and Analysis)
Outside Member

Abstract

The process of particle growth in a warm cloud caused by coalescence is studied. The purely probabilistic model introduced by Gillespie [J. Atmos. Sci. 29 (1972) 1496–1510] is used and solved exactly by the aid of the Monte Carlo algorithm developed by Gillespie [J. Atmos. Sci. 32 (1975) 1977–1989]. Another approach uses the kinetic coalescence equation which is solved numerically using finite difference methods. It is known that the stochastic completeness of the kinetic coalescence equation depends on the extent of correlations between particles. Our objective is to compare these two models and analyze the suitability of the kinetic coalescence equation to simulate the coalescence process using a Brownian diffusion collision kernel.

The stochastic coalescence model introduced by Gillespie is discussed in detail. A description of Gillespie's Monte Carlo simulation procedure and the numerical code

that implements this algorithm in Fortran are provided. This algorithm is applied to the coalescence kernel for Brownian diffusion and initial Poisson and uniform droplet size distributions. Numerical methods which can be applied to the continuous and the discrete forms of the kinetic equation are described. The discrete form of this equation is solved by using Euler's and the fourth order Runge-Kutta methods. Solutions from the two models at early and later times are examined and the effect of the number of droplets used in simulations is investigated. It is shown that solutions agree well for early and later times using large and relatively small number of droplets initially.

The problem of the growth of a large particle as it settles through a monodisperse suspension of small elemental particles is considered. It is demonstrated that the solution to the stochastic equation predicts about twice the growth rate of a large particle than the kinetic model.

To validate solutions obtained by the stochastic algorithm, the convergence of the solution to Poisson distribution as time increases is studied. It is shown that the normalized average concentration obtained from the initial uniform and Poisson distributions in the stochastic coalescence model can be approximated by the Marshall-Palmer distribution function well known in the cloud physics community.

The results of numerical simulations of the coalescence process using Brownian diffusion suggest that the kinetic equation in general produces an average size spectrum that well matches the stochastic average spectrum. However, in the case of

poorly mixed suspensions when correlations between particles are more important, these two models predict different size distributions, which is expected.

List of Figures

Chapter 1

Introduction

Clouds and precipitation play crucial roles in regulating Earth's energy balance and water cycle (Baker, 1997 [3]). It has been established that there are three basic physical processes (nucleation, condensation, and collection) involved in the formation of warm rain where the ice phase plays no role (Beard &Ochs, 1993 [5]; Jonas, 1996 [32], Telford, 1996 [58], Pinsky & Khain, 1997 [47]).

Nucleation is the process of initiation of a new phase in a supercooled (for liquid) or supersaturated (vapor) environment. In meteorology, particularly in cloud physics, the process of nucleation, i.e. the process by which cloud condensation nuclei initiate the phase change from vapor to liquid, is important in all cloud formation problems.

Condensation is the physical process by which a vapor becomes a liquid. Condensation in the atmosphere occurs by either of two processes: cooling of air to its

dewpoint, or addition of enough water vapor to bring the mixture to the point of saturation (that is, the relative humidity is raised to 100 percent). When either of these processes occurs, condensation ensues only if condensation nuclei or other surfaces are present. In the complete absence of such, condensation does not occur at nominal saturation. The spontaneous formation of liquid or solid droplets from water vapor (homogeneous nucleation) is opposed by the surface free-energy increase that attends the creation of new surfaces of the liquid or solid phase. Only for extreme supersaturation does this free-energy balance swing in favor of spontaneous nucleation [31].

Clouds form in the free atmosphere as a result of condensation of water vapor in rising currents of air, or by the evaporation of the lowest stratum of fog. The size of cloud drops varies from one cloud type to another, and within any given cloud there always exists a finite range of sizes [31]. Generally, cloud drops (droplets) range from $1 - 100\,\mu$m in diameter, and are very much smaller than raindrops. The occurence of collision and subsequent coalescence among cloud particles is called *collection* (Berry, 1967 [8]). Collection refers to the enhanced growth of those rare droplets large enough to have a gravitational fall speed that allows aggregation with smaller, typical cloud size droplets in the 10 μm radius range. Collision and coalescence originate from differential sedimentation, Brownian motion, laminar and turbulent shear, but differential sedimentation is the most important in warm clouds.

The problem, in cloud physics, of warm rain formation has drawn interest during the three to four last decades. It is generally understood that precipitation can be triggered by coalescence once a sufficient number of cloud droplets with radii larger than 20-25 μm are formed. Observations of rain from tropical cumulus whose tops had temperature above 0°C (Heywood, 1940 [28]; Mordy and Eber, 1954 [44]; Byers and Hall, 1955 [12]) has caused droplet collection to be labeled the "warm rain" process (Squires, 1955 [56]). But its importance extends to colder clouds. Braham, 1964 [11] found that droplets in supercooled summer cumulus over the central United States develop by the warm rain process before they freeze.

The collection is the process when the droplet grows by collecting other droplets. The phenomenon of collection occurs not only in meteorology when merging of drops in atmospheric clouds and aerosol transport (capture of aerosols by drops) are studied, but also in a wide range of other applications, e.g. in physics (aggregation of colloidal particles, growth of gas bubbles), chemistry (reacting polymers, soot formation) and astrophysics (formation of stars and planets). The survey papers by Aldous, 1999, [1] and Drake, 1972 [15] provide much more details. Processes of collection, coagulation, aggregation, or agglomeration are very similar in nature and they are described by the same equation that we introduce below. In this thesis, we study the process of collection.

Particle can be characterized by its radius, diameter, mass or volume. In the

thesis we will use volumes to identify particles. The time evolution of the average concentration of particles of a given size in some spatially homogeneous physical system is described by Smoluchowski's coalescence equation [63] (also called the kinetic coalescence equation)

$$\frac{\partial}{\partial t}c(t,x) = \frac{1}{2}\int_0^x K(x-y,y)c(t,x-y)c(t,y)dy - \int_0^\infty K(x,y)c(t,x)c(t,y)dy, \quad (1.1)$$

with initial condition

$$c(0,x) = c_0(x) \geq 0 \quad (1.2)$$

where $c(t,x)$ is the concentration of particles of type/volume x at time t. Here $t \geq 0$ and $x \geq 0$. Concentration of particles of size x increases as a result of coagulation or coalescence of particles of sizes $x-y$ and y. It decreases if particles of size x merge with any other particles. $K(x,y)$ is the collection coefficient or collection kernel that measures the rate of coalescence for particles of sizes x and y. It is non-negative, symmetric and represents properties of the physical medium. Equation (1.1) is called kinetic because it is the equation for the probability distribution of small particles.

If the particle's volume can take only discrete values $i = 1, 2, \ldots$, then the coagulation dynamics is governed by a discrete version of equation (1.1) where all integrals are replaced by sums. The discrete version of the coagulation equation is

$$\frac{\partial}{\partial t}c(t,i) = \frac{1}{2}\sum_{j=1}^{i-1} K(i-j,j)c(t,i-j)c(t,j) - \sum_{j=1}^{\infty} K(i,j)c(t,i)c(t,j) \qquad (1.3)$$

Both the continuous and the discrete equations have a wide range of applications in astrophysics, biology, chemistry, and meteorology.

There are many different mechanisms that bring two particles together: Brownian diffusion, gravitational sedimentation, free molecule collisions, turbulent motion of the host gas, acoustic waves, density, concentration and temperature gradients, particle electric charges, etc. The structure of the kernel $K(x,y)$ for different collision regimes is presented by Sabelfeld et al, 1996 [50] and Williams & Loyalka [64].

The coalescence equation (1.1) is a non-linear integro-differential equation. Despite significant interest in particle growth by coagulation, an exact solution for this equation has only been found for the simplest (and generally non-physical) cases (e.g. Golovin, 1963 [25]; Patil and Andrews, 1998 [46]; Lage, 2002 [35]; McCoy and Madras, 2003 [43]). Golovin, for example, found analytical solutions for kernels that do not depend on the particles' mass or for those that are proportional to the sum of the masses of the interacting particles. Analytical approximations can sometimes be derived for steady state solutions (Diemer and Olson, 2002 [14]). For more realistic kernel functions $K(x,y)$, for instance, the coalescence functions for various particle collision mechanism such as laminar shear, differential sedimentation, the coalescence equation cannot be solved analytically, and hence a numerical approach must be

taken.

There are several modes of coalescence modeling. They include the direct simulation of particle collisions, the numerical solution of the kinetic coalescence equation (1.1) and the exact Monte Carlo simulation of particle collisions. These simulation modes are complementary rather than competitive (Valioulis, 1986 [61]).

The justification for using the kinetic coalescence equation to describe the stochastic process was extensively treated in the literature [Scott, 1967 [51]; Scott, 1968 [52]; Gillespie, 1972, 1975 [23], [24] and Valioulis & List [60]]. It was shown that the kinetic coalescence equation (1.1) is indeed a good approximation to the fully stochastic collection process for typical cloud conditions. In addition, it has been established that the kinetic coalescence equation has validity only in the large droplet number limit, that is, when there are many droplets in the system (Laurenzi & Diamond, 2003 [36]). Consequently, the coalescence equation cannot predict the long-time behavior of the collection process when the particles or molecules completely aggregate or undergo a phase transition (Bayewitz et. al.,1974 [4], Lushnikov, 1978 [41]).

Great efforts were invested in developing numerical methods for simulating the coalescence process during the last three decades.

Moment methods. In these methods the overall particle spectrum is divided into discrete bins and the kinetic coalescence equation is transformed into a set of equations for moments in each bin. When the approximation uses only one moment, Blecks

method [9] is obtained. By approximating the distribution function with a power polynomial, using more than one moment, the multi-moments method is obtained by Tzivion et al. 1987, [59]. Other work using the method of moments includes papers by Frenklach, 1985 [21]; Frenklach and Harris, 1986 [20]; Grosschmidt et al., 2003 [27] and Angeli and Hewitt, 2000 [2]. In contrast to the discrete spectral point methods mentioned below, the moment methods exactly conserve total mass independently of the number of bins, time step, initial conditions, or kernel of interaction. The limitation of these methods relates to the fact that, by approximating the distribution function by moments, mass is distributed throughout the width of the bins that are otherwise not completely full. Therefore, during the early stages of coagulation, when the size distribution is narrow, moment methods will accelerate the coagulation process. The extent of this acceleration depends on the order of the polynomial used in the approximation in each bin and on the resolution (number of bins). Even though the method of moments is very efficient, it gives no information about the explicit shape of the distribution. In more complicated situations, there can also be problems with closure of the set of equations to be solved (Diemer and Olson, 2002 [13]).

Sectional or discrete points methods are a well established solution technique in coalescence process modelling. In these methods the overall particle distribution is represented by a number of discrete points, each having an equation which has been transformed from the kinetic coalescence equation. In order to calculate the collision

integrals it is necessary to prescribe the distribution function itself. Discretization of the size distribution can be linear (Hidy & Brock, 1970 [29]) or geometric (Gelbard & Seinfeld, 1978 [22]; Hounslow et al., 1988 [30]; Litster et al., 1995 [39]). Berry and Reinhardt, 1974 [6], [7], for example, formulated an approximation using a six-point Lagrangian polynomial. This method presents very good agreement with the analytical solution of Golovins kernel [25] using small time steps (13 sec). However, it does not satisfactorily conserve total mass for real kernels. Signeur et al., 1986 [54] published results from three different numerical methods: (a) discrete spectral points with cubic spline interpolation; (b) discrete spectral bins with an approximation of the distribution function, using only one moment; (c) a parameterization method. In their simulations the size of the particles was varied over a relatively narrow range. Under these conditions the coagulation process was very slow. Other works that also used a cubic spline approximation Eyre & Wright, 1988 [19], Gelbard & Seinfeld, 1978, [22] but for a broad spectrum and faster coagulation rate showed a significant lack of total mass conservation, even after short simulation times ($\approx$1020 min). Recent work includes efforts to use discretisation as a tool for recovering specific functionals of the distribution, rather than merely approximating the system (Kumar & Ramkrishna, 1996 [33]) and to use a varying particle size for each discrete interval in order to better account for nonuniformities in number density (Kumar & Ramkrishna, 1996 [34]). Several sectional approaches have been examined and reviewed

by Vanni, 2000 [62]. An alternative strategy is to employ *finite-element methods*, in which the solution is approximated as linear combinations of basis functions over a finite number of subdomains. Finite element methods include the *method of weighted residuals*, the *method of orthogonal collocation* and *Galerkin methods*. Nicmanis and Hounslow (1998) [45] applied a finite-element method to various cases of the steady state coalescence equation, finding more accurate solution than using the discretisation method and using less computational power. Liu and Cameron, 2001 [40], in a similar vein, used a *wavelet* based method. They found particular success in cases where steep fronts in the distribution are present, whereas discretisation in other solution methods would have to address this problem directly. *Stochastic (or Monte Carlo) methods* are an attractive way of tackling the coalescence equation due to the discrete nature of the mechanisms being modelled: breakage and coalescence (Ramkrishna, 1981 [48]). They can also provide a feasible solution method for multi-dimensional (dependent on more than just size) problems, where standard numerical techniques can become prohibitively computationally expensive. Broadly speaking, stochastic simulation involves generating fictitious realisations of the behaviour of a set of particles. This particle ensemble is an approximation of the real life system being examined. As the process relies on random number generation to choose the nature and timing of the coalescence and breakage events, many trajectories are generated, and an average (which converges to the solution of the population balance

equation (Eibeck and Wagner, 2000 [16])) is calculated. For the one-dimensional case (size dependency only), direct stochastic simulation (e.g. Gillespie, 1972 [23]) can be outperformed by conventional numerical techniques. The disadvantage of the direct method is that for simulating the evolution of the distribution function it is necessary to maintain, during all stages of the simulation, a large number of particles in the volume. This requires extremely large memory and computing time. For this reason this method is not very useful. A modification to the Monte-Carlo method was suggested by Seesselberg et al. [53]. Even though this proposed method significantly reduces the amount of computer memory required, it requires large computation time and, therefore, it is not useful even for one-dimensional models. Hence, there are several ways of improving the efficiency of simulation. To avoid the problems of decreasing particle number (and therefore variance increase) or increasing particle number (and thereby reduced efficiency), a particle combining technique can be employed, in which parallel arrays of particles are periodically combined to give an array with the desired number of particles (Sabelfeld etal., 1996 [50]). A natural extension of this technique is the constant number simulation method of Matsoukas and co-workers (Smith and Matsoukas, 1998 [55]; Lee and Matsoukas, 2000 [37]; Lin et al., 2002 [38]). One of the major inefficiencies of simulation comes from the coalescence process. A direct consideration of $\frac{1}{2}n(n-1)$ possible particle pairs (out of n particles) can be avoided by introducing the fictitious jump technique of Eibeck and Wagner (2000a,b) [16],

[17] . Here a majorant kernel is used that enables independent generation of the two coalescing particles. Babovsky (1999) considered a method for variance reduction by considering mass (rather than number) concentration. This mass flow technique has been used by Eibeck and Wagner, 2001 [18] to develop a stochastic algorithm that enables accurate simulation with far fewer stochastic particles in the simulation array.

In the thesis, we investigate the process of particle growth in a cloud, caused by coalescence, and rely on two models to address this issue: the kinetic equation and the purely probabilistic model, introduced by Gillespie, 1972 in [23] which is solved exactly by the aid of the Monte Carlo algorithm developed by Gillespie in 1975 and presented in [24].

The thesis is comprised of an abstract, this introduction chapter, five other chapters, a conclusion chapter and the bibliography. In the next chapter we discuss in more detail the stochastic coalescence process introduced and described in Gillespie's paper [23]. In chapter three we provide a description of Gillespie's Monte Carlo simulation procedure and the numerical code, implementing this algorithm in Fortran. We apply an algorithm to the coalescence kernel for Brownian diffusion and initial Poisson and uniform droplet size distributions. The fourth chapter contains a description of some numerical methods that can be applied to the continuous and the discrete forms of the kinetic equation. Also in this chapter we solve the discrete form of this equation by Euler's and the fourth order Runge-Kutta methods. The fifth chapter

provides an analysis of numerical results obtained in the third and forth chapters of the thesis and their comparison. We study the short and long time evolution of the average concentration. We also investigate the influence of the number of particles used in numerical simulations. We show that solutions agree well for early and later time as well as for large and not very large numbers of particles in the system initially. Then we study the growth of a large particle as it falls through monodisperse set of smaller particles according to the two models and demonstrate that the solution to the stochastic equation predicts a higher growth rate of the large particle. We discuss why the kinetic model does not agree with the stochastic model by referring to the assumptions that were used to derive the kinetic model. In the last chapter we investigate the convergence of the solution to Poisson distribution as time increases and show that normalized average concentration obtained from the initial uniform and Poisson distributions in the stochastic coalescence model can be approximated by the Marshall-Palmer distribution function [42] , well known in the cloud physics community.

Chapter 2

The Stochastic Coalescence Model for Droplet Growth in Warm Clouds

2.1 The stochastic coalescence model of Gillespie

The process of rain formation in warm clouds can be split into two major stages. During the first stage, cloud droplets form and grow thanks to condensation of water vapor around nuclei. Growth by condensation proceeds until production of supersaturation ends. This normally does not happen in clouds if there are positive updrafts, i.e. vertical movements of air upward. After the droplets reach some critical size, particles start also growing by collection with other particles and the growth by con-

densation becomes less important. Larger particles collide with and collect smaller ones and grow until they reach the size of rain droplets and fall to the ground as precipitation. Here we are interested in this second stage, i.e. the growth of cloud particles to rain droplets by the collection process, also called the "coalescence process". In this chapter we describe in great detail the stochastic coalescence model for rain formation in warm clouds following Gillespie [23]. We begin by describing the probabilities of particle growth history via processes of collision and coalescence in the cloud. The physical situation assumes a cloud of fixed volume wherein droplets of all sizes are uniformly and randomly distributed in the cloud at $t = 0$ and remain so for all $t > 0$.

Given that liquid water is incompressible and assuming that all cloud and rain droplets are spherical, a given droplet can be represented either by its mass, its volume or its radius. However, it is convenient to specify the size of a droplet by the discrete number m of water molecules it contains. So we define an

$$"m - \text{droplet}" \equiv \text{a droplet which contains exactly } m \text{ molecules}, \tag{2.1}$$

where m can be any positive integer.

Since we cannot predict exactly how many droplets of a particular size we have at any time $t > 0$, the process of particle growth is described in a strictly probabilistic way. The random mechanism can be defined by the function $C(m_1, m_2; t)$, which we assume exists, called the "coalescence kernel" or simply the "coalescence probability

function", defined by

$$C(m_1, m_2; t)\delta t \equiv \text{probability that an arbitrary } m_1 - \text{droplet will coalesce with an arbitrary } m_2 - \text{droplet in the time interval } (t, t+\delta t). \tag{2.2}$$

The time interval δt is sufficiently small that we do not need to account for the possibility that, during δt, the m_1-droplet or the m_2-droplet may also be involved in collection events other than that event to which (2.2) refers.

The coalescence probability function allows to predict the probability of finding a given number of droplets of a particular size at time t. This suggests that appropriate functions describing the state of the cloud in the stochastic model are the functions

$$P(n, m; t) \equiv \text{probability that there are exactly } n \ m - \text{droplets in the cloud at time } t. \tag{2.3}$$

These are functions of n, in which m and t appear as parameters; since it is a probability, its values always lie between 0 and 1.

In Probability Theory the mathematical expectation, or mean, of the random variable n is

$$N(m; t) = \sum_{n=0}^{\infty} nP(n, m; t). \tag{2.4}$$

So $N(m; t)$ defines the average or expected number of m-droplets in the cloud at time t and it is also the first moment of the probability distribution function with respect to n since the kth moment or the mathematical expectation of magnitude n^k is defined by

$$N_k(m; t) = \sum_{n=0}^{\infty} n^k P(n, m; t). \tag{2.5}$$

The expected value $N(m;t)$ of a random variable n is of special interest because it describes where the probability distribution is centered. By itself, however, the mean does not give an adequate description of the shape of the distribution. It is also important to know how the observations fluctuate from the mean. For this the variance of n is used, defined as

$$\triangle^2(m;t) = N_2(m;t) - N^2(m;t). \tag{2.6}$$

The quantity $\triangle(m;t)$ is the standard deviation of an observation from its mean.

2.2 The time-evolution equations

Following [23], we derive a time-evolution equation for $P(n,m;t)$ in (2.3), considering this quantity at two moments of time, t and $t+\delta t$. In a short time δt any two particles can coalesce with probability $C\delta t$. Recall that we have chosen δt to be sufficiently small so that during the time interval $(t, t+\delta t)$ there could be at most one coalescence.

There are three different ways in which the number of m-droplets can change during the period of time δt [23]:

1) One m-droplet can be created by the coalescence of an m'-droplet and $m-m'$ droplet, where $m' < m$;

2) One m-droplet can be removed by the coalescence of an m-droplet and an m'-droplet, where $m' \neq m$;

3) Two m-droplets can be removed by the coalescence of two m-droplets.

We can write $P(n,m;t+\delta t)$ as the sum of the probabilities of the following four mutually exclusive eventualities, consisting in having exactly n m-droplets at time $t+\delta t$ and taking into account the case when no m-droplets will be created or destroyed for the short period of time δt [23]:

$$\begin{aligned}
P(n,m;t+\delta t) = P(n,m;t) \times \{&\text{probability that, given } n \text{ } m\text{-droplets at } t,\\
&\text{no } m\text{-droplets will be created or destroyed in } (t,t+\delta t)\}+\\
+P(n-1,m;t) \times \{&\text{probability that, given } n-1 \text{ } m\text{-droplets at } t, \text{ one } \bar{m}\text{-}\\
&\text{droplet will be created in } (t,t+\delta t)\}+\\
+P(n+1,m;t) \times \{&\text{probability that, given } n+1 \text{ } m\text{-droplets at } t, \text{ one } m\text{-}\\
&\text{droplet will be destroyed in } (t,t+\delta t)\}+\\
+P(n+2,m;t) \times \{&\text{probability that, given } n+2 \text{ } m\text{-droplets at } t, \text{ two } m\text{-}\\
&\text{droplets will be destroyed in}(t,t+\delta t)\}. \qquad (2.7)
\end{aligned}$$

As we know that the sum of probabilities of the events which create the full group equals to 1, the quantity in braces in the first term of (2.7) can be written as [23]:

$$\begin{aligned}
&\{\text{probability that no } m\text{-droplets will be created or destroyed in}(t,t+\delta t)\}\\
&= 1 - \{\text{probability that one } m\text{-droplet will be created in}(t,t+\delta t)\}\\
&\quad -\{\text{probability that one } m\text{-droplet will be destroyed in}(t,t+\delta t)\}\\
&\quad -\{\text{probability that two } m\text{-droplets will be destroyed in}(t,t+\delta t)\}.
\end{aligned}$$

Inserting this into (2.7) and rearranging terms, we obtain the following equation [23]:

$$P(n,m;t+\delta t)-P(n,m;t)=P(n-1,m;t)\times\{\text{probability that, given } n-1 \text{ } m\text{-droplets at } t, \text{ one } m\text{-droplet will be created in } (t,t+\delta t)\}-$$
$$-P(n,m;t)\times\{\text{probability that, given } n \text{ } m\text{-droplets at } t, \text{ one } m\text{-droplet will be created in } (t,t+\delta t)\}+$$
$$+P(n+1,m;t)\times\{\text{probability that, given } n+1 \text{ } m\text{-droplets at } t, \text{ one } m\text{-droplet will be destroyed in } (t,t+\delta t)\}-$$
$$-P(n,m;t)\times\{\text{probability that, given } n \text{ } m\text{-droplets at } t, \text{ one } m\text{-droplet will be destroyed in } (t,t+\delta t)\}+$$
$$+P(n+2,m;t)\times\{\text{probability that, given } n+2 \text{ } m\text{-droplets at } t, \text{ two } m\text{-droplets will be destroyed in } (t,t+\delta t)\}-$$
$$-P(n,m;t)\times\{\text{probability that, given } n \text{ } m\text{-droplets at } t, \text{ two } m\text{-droplets will be destroyed}(t,t+\delta t)\}. \tag{2.8}$$

Looking at the factors in braces on the right side of (2.8), we recognize that each of them is a probability for a particular kind of coalescence to take place in $t, t+\delta t$. The next step is to derive explicit mathematical expressions for the quantities in braces. For this two kinds of conditional probabilities (2.9), (2.10) and the coalescence function (2.2) are required. We define

$$P(n,m|n',m';t)\equiv\text{probability that, at time } t, \text{ there are exactly } n \text{ } m-\text{droplets in the cloud, given that there are already exactly } n' \text{ } m'\text{-droplets in the cloud,} \tag{2.9}$$

$P(n, m|n', m'; n'', m''; t) \equiv$ probability that, at time t, there are exactly n $m-$ droplets in the cloud, given that there are already n' m'-droplets and n'' $m''-$ droplets in the cloud. (2.10)

These are called the "singly conditional" probability (2.9) and the "doubly conditional" probability (2.10) [23].

Consider the case when, given $n+1$ m-droplet at time t, one m-droplet will be destroyed during the time δt. The probability for having n' m'-droplets, given that there are $n+1$ m-droplets, is $P(n', m'|n+1, m; t)$. The probability of an (m, m') coalescence for this particular configuration is

$$(n+1)n' \times C(m, m'; t)\delta t.$$

The total probability of an (m, m') coalescence in $(t, t+\delta t)$, given $n+1$ m-droplets, is then

$$(n+1) \sum_{\substack{m'=1 \\ m' \neq m}}^{\infty} \sum_{n'=1}^{\infty} n' P(n', m'|n+1, m; t) C(m, m'; t)\delta t. \tag{2.11}$$

By using essentially the same kind of logic, we can find the explicit expressions for each quantity in braces in (2.8). For the case when, given n m-droplets at time t, one m-droplet will be destroyed during the time δt we have the following expression

$$n \sum_{\substack{m'=1 \\ m' \neq m}}^{\infty} \sum_{n'=1}^{\infty} n' P(n', m'|n, m; t) C(m, m'; t)\delta t. \tag{2.12}$$

The probability that, given $n+2$ m-droplets at t, two m-droplets will be destroyed by the coalescence of two m-droplets during δt is

$$\frac{1}{2}(n+2)(n+1)C(m, m; t)\delta t. \tag{2.13}$$

The probability that two m-droplets will be destroyed by the coalescence of two droplets of mass m in $(t, t+\delta t)$, given that there are already n m-droplets in the cloud at time t is

$$\frac{1}{2}n(n-1)C(m,m;t)\delta t. \tag{2.14}$$

Recall that one m-droplet can be created only by the coalescence of some m'-droplet and an $(m-m')$-droplet, where $m' < m$. So we need to consider two cases according to whether the coalescence is between different size droplets (i.e.,$m' \neq m - m'$) or like-sized droplets (i.e.,$m' = m - m' = m/2$). The total probability for the creation of an m-droplet by the coalescence of two unlike droplets during the time δt, given that there are $n-1$ m-droplets is

$$\frac{1}{2}\sum_{\substack{m'=1 \\ m'\neq\frac{m}{2}}}^{m-1}\sum_{n'=1}^{\infty}\sum_{n''=1}^{\infty} n'n''P(n',m'|n-1,m;t)\times P(n'',m-m'|n-1,m;n',m';t)\times$$

$$\times C(m',m-m';t)\delta t. \tag{2.15}$$

and the probability for the creation of an m-droplet by the coalescence of two like droplets in $(t, t+\delta t)$, given that there are already $n-1$ m-droplets, is

$$\varepsilon(m)\frac{1}{2}\sum_{n'=1}^{\infty} n'(n'-1)\times P(n',\frac{m}{2}|n-1,m;t)C(\frac{m}{2},\frac{m}{2};t)\delta t$$

where

$$\varepsilon(m) = \begin{cases} 1, & \text{if } m \text{ is even} \\ 0, & \text{if } m \text{ is odd} \end{cases}$$

for this case to occur. The quantity for the creation of one m-droplet, given that there exist n m-droplets in the cloud at time t differs from the expression just shown only by the presence of n, instead of $n-1$, m-droplets at time t. If we substitute all

mathematical expressions for the probabilities for the particular kind of coalescence to occur in $(t, t+\delta t)$, divide through by δt and take the limit $\delta t \to 0$, we obtain an expression for $\partial P(n,m;t)/\partial t$. But it is not possible to solve this equation, since it contains, in addition to $P(n,m;t)$ and $C(m_1,m_2;t)$, the unknown conditional probabilities (2.9) and (2.10). There appears to be no way of continuing without making simplifying assumptions. The simplest way of proceeding is to neglect correlations among the droplet population probabilities, [23]:

$$P(n,m|n',m';t) \approx P(n,m;t) \;\; for \;\; m \neq m', \tag{2.16}$$

$$P(n,m|n',m';n'',m'';t) \approx P(n,m;t) \;\; for \;\; m \neq m' \neq m''. \tag{2.17}$$

Introducing these approximations into the expressions for the probabilities in (2.8), performing the n' and n'' summations with the aid of (2.4) and (2.5), dividing through by δt and taking the limit $\delta t \to 0$ the following time-evolution equation for the probability distribution function is obtained [23]:

$$\frac{\partial P(n,m';t)}{\partial t} = [P(n-1,m;t) - P(n,m;t)] \times \Big\{ A(m;t) + \frac{\varepsilon(m)}{2}[\Delta^2(\frac{m}{2};t) - N(\frac{m}{2};t)]$$
$$\times C(\frac{m}{2},\frac{m}{2};t) \Big\} + [(n+1)P(n+1,m;t) - nP(n,m;t)] \times [B(m;t) - N(m;t)C(m,m;t)]$$
$$+[(n+1)(n+2)P(n+2,m;t) - (n-1)nP(n,m;t)] \times \frac{1}{2}C(m,m;t), \tag{2.18}$$

where $\Delta^2(m;t)$ is the variance of the probability distribution function and for simplicity the following abbreviations were introduced [23]

$$A(m;t) \equiv \frac{1}{2}\sum_{m'=1}^{m-1} N(m';t)N(m-m';t)C(m',m-m';t), \tag{2.19}$$

$$B(m;t) \equiv \sum_{m'=1}^{\infty} N(m';t)C(m,m';t). \tag{2.20}$$

From (2.5) we have

$$\frac{\partial}{\partial t}N_k(m;t) = \sum_{n=0}^{\infty} n^k \frac{\partial}{\partial t}P(n,m;t).$$

Inserting for $\partial P/\partial t$ the expression on the right side of (2.18), and using the relations

$$\sum_{n=0}^{\infty} n^k P(n-1,m;t) = \sum_{n=0}^{\infty}(n+1)^k P(n,m;t),$$

$$\sum_{n=0}^{\infty} n^k (n+1) P(n+1,m;t) = \sum_{n=0}^{\infty}(n-1)^k n P(n,m;t),$$

$$\sum_{n=0}^{\infty} n^k (n+1)(n+2) P(n+2,m;t) = \sum_{n=0}^{\infty}(n-2)^k (n-1) n P(n,m;t),$$

we obtain the evolution equations for all the k^{th} moments $N_k(m;t)$ of $P(n,m;t)$ [23].

$$\frac{\partial N_k(m;t)}{\partial t} = \sum_{n=0}^{\infty}[(n+1)^k - n^k]P(n,m;t) \times \Big\{A(m,t) + \frac{\varepsilon(m)}{2}[\Delta^2(\frac{m}{2};t) - N(\frac{m}{2};t)]$$

$$\times C(\frac{m}{2},\frac{m}{2};t)\Big\} - \sum_{n=0}^{\infty}[n^{k+1} - (n-1)^k n]P(n,m;t) \times [B(m,t) - N(m,t)C(m,m;t)]$$

$$- \sum_{n=0}^{\infty}[(n-1)n^{k+1} - (n-2)^k (n-1)n]P(n,m;t) \times \frac{1}{2}C(m,m;t). \qquad (2.21)$$

In particular, when $k = 1$ we have

$$\frac{\partial N(m;t)}{\partial t} = A(m;t) - N(m;t)B(m;t) + \frac{\varepsilon(m)}{2}C(\frac{m}{2},\frac{m}{2};t)[\Delta^2(\frac{m}{2};t) - N(\frac{m}{2};t)]$$

$$-C(m,m;t)[\Delta^2(m;t) - N(m;t)]. \qquad (2.22)$$

This is the evolution equation for the expected number of m-droplets in the cloud at time t. But it is not closed, since it contains the second moment of $P(n,m;t)$. We have to make another assumption to close this equation.

2.3 The case $C(m,m;t) \equiv 0$ and long time Poisson distribution

The equation would simplify considerably if $C(m_1, m_2)$ were identically zero whenever $m_1 = m_2$. Evidently this is the condition which means that the probability for two droplets of the same mass to coalesce is prohibited. In a real cloud due to enormous range of cloud droplet sizes this condition is approximately satisfied since two droplets of the same mass falling with the same terminal velocity are not likely to coalesce. But this reasoning is not valid in some particular cases, for instance in the case of Brownian motion. On the other hand we can assume that this condition is true on a different ground. For a real cloud $A(m;t)$ and $B(m;t)$, defined in (2.19) and (2.20), will contain an enormous number of terms. Therefore the contributions to the right hand side of the equation (2.18) from the terms which do not contain $A(m;t)$ or $B(m;t)$ will be negligible. But these terms are those which can be get rid of by assuming that $C(m_1, m_2) \equiv 0$. Under this condition the time-evolution equation for $P(n,m;t)$ becomes

$$\frac{\partial P(n,m;t)}{\partial t} = [P(n-1,m;t) - P(n,m;t)]A(m,t) + [(n+1)P(n+1,m;t) - n \times P(n,m;t)]B(m,t). \tag{2.23}$$

Equation (2.22) now becomes

$$\frac{\partial N(m;t)}{\partial t} = \frac{1}{2}\sum_{m'=1}^{m-1} N(m';t)N(m-m';t)C(m',m-m';t) - \sum_{m'=1}^{\infty} N(m;t)N(m';t)C(m,m';t), \tag{2.24}$$

and it is evidently the kinetic equation. In terms of the quantities $A(m,t)$ and $B(m,t)$ this equation can be written as

$$\frac{\partial N}{\partial t} = A - NB, \tag{2.25}$$

where the arguments m and t are suppressed for convenience. Under this condition the time-evolution equations for the second and third moments of $P(n,m;t)$ become

$$\frac{\partial N_2}{\partial t} = -2BN_2 + [A + N(2A+B)], \tag{2.26}$$

$$\frac{\partial N_3}{\partial t} = -3BN_3 + [A + N(3A-B) + 3N_2(A+B)]. \tag{2.27}$$

An equation for N_k can be obtained from (2.21) by using the binomial expansion and (2.4) to express the quantities in (2.21) as linear combinations of the functions $N_k(m;t)$. In the case when $C(m,m;t) \equiv 0$ it is

$$\frac{\partial N_k}{\partial t} = -kBN_k + \left\{A + N[kA + (-1)^k B] \right. \tag{2.28}$$
$$\left. + \sum_{j=2}^{k-1} N_j \left[\binom{k}{j} A - (-1)^{k-j} \binom{k}{j-1} B \right] \right\}, k \geq 3,$$

where (k,j) is the binomial coefficient. Since $\Delta^2 = N_2 - N^2$, an equation for $\frac{\partial \Delta^2}{\partial t}$ can be obtained, using (2.25) and (2.26) :

$$\frac{\partial \Delta^2}{\partial t} = \frac{\partial}{\partial t}(N_2 - N^2) = -2B[N_2 - N^2] + A + BN, \tag{2.29}$$

whence

$$\frac{\partial \Delta^2}{\partial t} = -2B\Delta^2 + [A + NB]. \tag{2.30}$$

The equations (2.26) and (2.30) become ordinary first-order linear differential equations once we have the solution to (2.25) and functions $A(m,t)$ and $B(m,t)$ from

(2.19) and (2.20). Recall two properties of the general first-order linear differential equation

$$\frac{dy}{dt} = -b(t)y + c(t) \tag{2.31}$$

First, its general solution is

$$y(t) = \exp\left(-\int_0^t b(t')\,dt'\right) \times \left[y(0) + \int_0^t c(t') \exp\left(\int_0^{t'} b(t'')\,dt''\right)\,dt'\right]. \tag{2.32}$$

Second, if $y_1(t)$ is a particular solution, then

$$y(t) - y_1(t) = [y(0) - y_1(0)] \exp\left(-\int_0^t b(t')\,dt'\right). \tag{2.33}$$

Equation (2.25) we can rewrite as

$$\frac{dN}{dt} = -2BN + [A + NB].$$

Comparing it with (2.30), we conclude that $N(m;t)$ is a particular solution of the equation for $\Delta^2(m;t)$. By (2.33) we have

$$\Delta^2(m;t) - N(m;t) = [\Delta^2(m;0) - N(m,0)] \times \exp\left(-2\int_0^t B(m,t')\,dt'\right). \tag{2.34}$$

To understand this result, the quantity $\mathcal{P}(m,t)$ needs to be introduced. It is defined as [23]

$$\mathcal{P}(m,t) \equiv \text{probability that a given } m-\text{droplet in the cloud at time } 0 \text{ will not suffer a coalescence in } (0,t). \tag{2.35}$$

If there are n' m'-droplets in the cloud at time t, then the probability that one of them will coalesce with the given m-droplet in time $(t, t+dt)$ is $n'C(m,m';t)dt$. Hence,

Probability that an m-droplet will suffer a coalescence in $(t, t+dt)$

$$= \sum_{m'=1}^{\infty} \sum_{n'=1}^{\infty} [P(n', m'; t)][n' C(m, m'; t) dt] = \sum_{m'=1}^{\infty} N(m'; t) C(m, m'; t) dt$$

$$\equiv B(m, t) dt,$$

where (2.4) and (2.20) were used. Now we can write

$$\mathcal{P}(m, t+dt) = \mathcal{P}(m, t) \times [1 - B(m, t) dt]$$

from where $\dfrac{d\mathcal{P}(m,t)}{\mathcal{P}(m,t)} = -B(m,t)dt$. So

$$\mathcal{P}(m, t) = \exp\left(- \int_0^t B(m, t')\, dt' \right). \tag{2.36}$$

Therefore (2.34) can be written

$$\Delta^2(m; t) - N(m; t) = [\Delta^2(m; 0) - N(m, 0)] \mathcal{P}^2(m, t) \tag{2.37}$$

As the time progresses the chance for the droplet to escape coalescence reduces so we will not be mistaken if we expect that

$$\mathcal{P}(m, t) \longrightarrow 0 \quad \text{as} \quad t \longrightarrow \infty \tag{2.38}$$

Combining this with (2.37) gives us that

$$\Delta^2(m; t) \longrightarrow N(m; t) \quad \text{as} \quad t \longrightarrow \infty \tag{2.39}$$

If we assign $\mathcal{P}(m, \tau_m)$ to be $\frac{1}{2}$ defining τ_m as the solution to the equation

$$\int_0^{\tau_m} B(m, t)\, dt = \log 2, \tag{2.40}$$

then it is clear from (2.37) that τ_m is the time for the difference between $\Delta^2(m;t)$ and $N(m;t)$ to reduce to one-fourth of its initial value.

We have proved that the variance of the probability distribution function approaches its mean [23]. (2.37) can be written in the form

$$N_2(m;t)-[N^2(m;t)+N(m;t)] = \{N_2(m;0)-[N^2(m;0)+N(m;0)]\}\mathcal{P}^2(m;t). \quad (2.41)$$

The first two moments with respect to n of the Poisson function

$$P^*(n,m;t) \equiv \frac{e^{-N(m;t)}N^n(m;t)}{n!} \quad (2.42)$$

are given by

$$\begin{aligned} N_1^*(m;t) &= N(m;t) \\ N_2^*(m;t) &= N^2(m;t)+N(m;t) \end{aligned} \quad (2.43)$$

So we can conclude that the second moment $N_2(m;t)$ of $P(n,m;t)$ approaches the second moment $N_2^*(m;t)$ of the Poisson function as time increases. In order to prove that $P(n,m;t)$ approaches $P^*(n,m;t)$ it is necessary to show that $N_k(m;t)$ approaches $N_k^*(m;t)$ for $k=3,4...$ as well [23]. By differentiating (2.42) with respect to t and using (2.25) it can be shown that $P^*(n,m;t)$ satisfies the time-evolution equation (2.23) for $P(n,m;t)$. Consequently the moments $N_k^*(m;t)$ of $P^*(n,m;t)$ satisfy the same equations as the corresponding moments $N_k(m;t)$ of $P(n,m;t)$. From (2.28) and the fact that $N_1^* = N$ we have

$$\begin{aligned} \frac{\partial N_k^*}{\partial t} &= -kBN_k^* + \{A + N[kA+(-1)^k B] \\ &+ \sum_{j=2}^{k-1} N_j^* \left[\binom{k}{j}A - (-1)^{k-j}\binom{k}{j-1}B\right]\Big\}, k \geq 3, \end{aligned} \quad (2.44)$$

If we now define the difference

$$D_k(m;t) \equiv N_k(m;t) - N_k^*(m;t) \tag{2.45}$$

and then subtract (2.44) from (2.28) we obtain the following time-evolution equation for $D_k(m;t)$:

$$\frac{\partial D_k}{\partial t} = -kBD_k + \sum_{j=2}^{k-1} F_{kj} D_j, \quad k \geq 3. \tag{2.46}$$

where F_{kj} are defined as

$$F_{kj}(m;t) \equiv \binom{k}{j} A(m;t) - (-1)^{k-j} \binom{k}{j-1} B(m;t).$$

Equation (2.46) is a first-order linear differential equation. Its general solution can be written using (2.32) and (2.36) as

$$D_k(m;t) = \mathcal{P}^k(m;t)[D_k(m;0) + \int_0^t \sum_{j=2}^{k-1} F_{kj}(m,t') D_j(m;t') \mathcal{P}^{-k}(m;t')\, dt'], \quad k \geq 3. \tag{2.47}$$

From (2.41) $D_2(m;t) = D_2(m;0)\mathcal{P}^2(m;t)$. Therefore for $k = 3$ the equation (2.47) yields

$$D_3(m;t) = \mathcal{P}^3(m;t)[D_3(m;0) + \int_0^t F_{32}(m,t') D_2(m;0) \mathcal{P}^2(m;t') \mathcal{P}^{-3}(m;t')\, dt'].$$

Since $\mathcal{P}(m;t) \longrightarrow 0$ as time progresses, then for large t we have

$$D_3(m;t) \sim O(\mathcal{P}^3(m;t)) + O(\mathcal{P}^2(m;t)) \sim O(\mathcal{P}^2(m;t)),$$

from where we can conclude that as $t \longrightarrow \infty$, $D_3(m;t) \longrightarrow 0$ as fast as $\mathcal{P}^2(m;t) \longrightarrow 0$. If $D_2(m;t), D_3(m;t), ..., D_{k-1}(m;t)$ all approach zero as $\mathcal{P}^2(m;t)$, then (2.47) yields

that for large t,

$$D_k(m;t) \sim \mathcal{P}^k(m;t)[D_k(m;0) + \int_0^t \sum_{j=2}^{k-1} F_{kj}(m,t')O(\mathcal{P}^2(m;t'))\mathcal{P}^{-k}(m;t')\,dt'],$$

$$\sim O(\mathcal{P}^k(m;t)) + O(\mathcal{P}^2(m;t)) \sim O(\mathcal{P}^2(m;t)).$$

Therefore for all $k \geq 2$, $D_k(m;t)$ approaches zero, so $N_k(m;t)$ approaches $N_k^*(m;t)$ as fast as $\mathcal{P}^2(m;t) \longrightarrow 0$.

This means that as $t \longrightarrow \infty$ the probability distribution function $P(n,m;t)$ will be approaching a Poisson distribution in n and the time for this approach is given by

$$\int_0^{\tau_m} B(m,t)dt = \log 2.$$

Chapter 3

Monte Carlo Simulation Procedure

Gillespie in his paper [24] outlined the rigorous method for numerically simulating the stochastic coalescence process in a cloud. This algorithm, which is a "Monte Carlo simulation" procedure, allows to study an evolution in time of an initially specified droplet size distribution and produce numerical estimates of the fluctuations in the developing droplet size spectrum. In this chapter we are going to implement the algorithm , apply it to a specific coalescence kernel and specific initial droplet volume distributions. Now we will give the description of the procedure. Suppose that at time t there are N droplets in the cloud. Label the droplets by index i, (i=1,...,N) and let X_i denote the size of the droplet. Define the "coalescence probability density function" $P(\tau, i, j)$ which has the property that

$$P(\tau, i, j) \equiv \text{probability at time } t \text{ that the next coalescence will occur in the time interval } (t+\tau, t+\tau+d\tau), \text{and will be the coalescence of droplets } i \text{ and } j \quad (i<j) \tag{3.1}$$

The expression for this function which Gillespie derived in [24], considering the probability (3.1) as a product of three probabilities, forms the basis for the simulation algorithm. This expression is

$$P(\tau, i, j) = C_{ij} \exp[-\sum_{k=1}^{N-1} \sum_{l=k+1}^{N} C_{kl}\tau]. \tag{3.2}$$

Here $C_{kl} \equiv C(X_k, X_l)$ where $k = 1, 2, ..., N-1$; $l = k+1, k+2, ..., N$. These limits imply that the index pair (k, l), where $k < l$, uniquely labels each of the $N(N-1)/2$ distinct pairs of cloud droplets. Just to remind that $C(X_k, X_l)$ is a function, called the "coalescence kernel", which has the property that

$$C_{kl}d\tau \equiv \text{probability that droplets } k \text{ and } l \text{ will coalesce in the next infinitesimal time interval } d\tau. \tag{3.3}$$

The simulation algorithm is as follows [24]:

1. Specify the masses(or volumes) $X_1, X_2, ...X_N$ of all N droplets at the time $t = 0$ and a series of "sample times", including t_{stop}.

2. Calculate $N(N-1)/2$ elements C_{kl} according to the coalescence kernel $C(X_k, X_l)$; $k = 1, 2, ..., N-1$, $l = k+1, k+2, ..., N$.

3. Generate a random triplet (τ, i, j) according to the density function (3.2) by one of the methods proposed by Gillespie in [24]. We have chosen to apply a full-conditioning method. This method is comprised of writing the three-variable density function (3.2) as the product of three one-variable density functions:

$$P(\tau, i, j) = P_1(\tau)P_2(i|\tau)P_3(j|\tau, i). \tag{3.4}$$

The physical significance of the quantities on the right side of (3.4) are that $P_1(\tau)d\tau$ is the probability that the next coalescence will happen between times $t+\tau$ and $t+\tau+d\tau$, irrespective of which droplets coalesce; $P_2(i|\tau)$ is the probability that the next coalescence will involve the droplet i, given that it occurs at time $t+\tau$, but irrespective of which another droplet is involved; $P_3(j|\tau,i)$ is the probability that the next coalescence will involve droplet j, given that it occurs at time $t+\tau$ and involves droplet i. The expressions for density functions P_1, P_2, P_3 are as follows:

$$P_1(\tau) = C_0 \exp(-C_0\tau)), \;\; 0 \leq \tau < \infty, \tag{3.5}$$

$$P_2(i|\tau) = P_2(i) = C_i/C_0, \;\; i = 1, ..., N-1, \tag{3.6}$$

$$P_3(j|\tau, i) = P_3(j|i) = C_{ij}/C_i, \;\; j = i+1, ..., N, \tag{3.7}$$

where

$$C_i \equiv \sum_{j=i+1}^{N} C_{ij}, \;\; i = 1, ..., N-1, \tag{3.8}$$

$$C_0 \equiv \sum_{i=1}^{N-1} C_i \equiv \sum_{i=1}^{N-1} \sum_{j=i+1}^{N} C_{ij}. \tag{3.9}$$

The product of the three quantities (3.5), (3.6) and (3.7) gives the quantity in (3.2). Also each of the functions in (3.5), (3.6) and (3.7) satisfies probability normalization requirement, i.e.,

$$\int_0^\infty P_1(\tau)\, d\tau = \int_0^\infty \exp(-C_0\tau) C_0\, d\tau = 1,$$

$$\sum_{i=1}^{N-1} P_2(i) = \sum_{i=1}^{N-1} C_i/C_0 = 1,$$

$$\sum_{j=i+1}^{N} P_3(j|i) = \sum_{j=i+1}^{N} C_{ij}/C_i = 1.$$

3.1 Generate a random number τ according to $P_1(\tau)$ in (3.5) by the inversion method.

For this take out a random number r_1 from the uniform random number generator and then choose for τ the value that satisfies $F(\tau) = r_1$ where F is the probability distribution function corresponding to the probability density function $P(\tau)$ and is defined by

$$F(\tau) \equiv \int_0^{\tau} P(\tau')\, d\tau', \quad 0 \leq \tau < \infty.$$

So in our case

$$\tau = C_0^{-1} \ln(1/r_1). \tag{3.10}$$

3.2 Generate a random integer i according to $P_2(i)$ in (3.6) and a random integer j according to $P_3(j|i)$ in (3.7).

Pick a second random number r_2 from the uniform distribution in the unit interval and take i to be that integer for which

$$\sum_{i'=1}^{i-1} C_{i'} < r_2 C_0 \leq \sum_{i'=1}^{i} C_{i'}. \tag{3.11}$$

Pick a third random number r_3 from the uniform distribution in the unit interval and take j to be that integer for which

$$\sum_{j'=i+1}^{j-1} C_{ij'} < r_3 C_i \leq \sum_{j'=i+1}^{j} C_{ij'}, \tag{3.12}$$

where i is the value found in (3.11).

4. Advance t by τ, remove droplets i and j, insert a new droplet of mass $X_i + X_j$. Adjust the droplet numbering scheme to reflect the fact that there is one less droplet than before in the cloud.

5. If t has been advanced through one of the sample times, display the droplet mass spectrum at this time or evaluate and display the specific properties of the droplet mass distribution which are being studied. If $t \geq t_{stop}$ or if only one droplet remains, terminate the calculation. Otherwise, return to step 2.

Next we present the implementation of this algorithm in Fortran.

```
program algorithm ! .and.(counter -1 /= 0)

   implicit none
   real :: PR,Rndom
   integer,parameter::M=100,absT=283, V = 2000
   real,parameter::Bltz=1.38,mu=1.307
   integer :: counter, PV,i,j,EoF,X(M),WX(M),NofV(V),
              in_distr(M),N,k,l,p,q,Aux,number=0, RUN,Aver(M),UV
   integer :: i1, i2, i3, i4,j1,j4,ip,jp,
              num_output,ISEED, N1, E,curr_dr,N2=0,Fmax
   !real,parameter::delta=0.00001
   real::Im(M), Xmin,F(M),lambda,C(M,M),Z(M-1)=0.0,Z_0=0.0,
   Fmin,T=0.0,S=0.0, A=0.0,B=0.0,C_0=0.013, N_av(V),Momnt(V),
   St_dev(V),var(V),Average1,Average2,
   in_aver(M),mean,mean2,smomnt,sum3=0.0,variance,sum1=0.0,
```

```
   sum2=0.0,VL
   double precision::Pi,tau,time=0.0,r_1,r_2,r_3, tMax = 0.1,
   U,DUNI,DUSTAR,USEED
   intrinsic::exp,Log
   logical::istat=.False.,jstat=.False.
   CHARACTER*4::BUFFER
   PR=1
   lambda=10.0
   Pi=4*Atan(1.0)

ISEED=305
USEED=DUSTAR(ISEED)
U=DUNI()
N=M
N1=1500
!N1=2000
!N1=10100
E=0
!curr_dr=0

do i1=1,N1
   N_av(i1)=0.0
   Momnt(i1)=0.0
```

```
   St_dev(i1)=0.0
enddo

Do RUN = 1, 1000
print*,'Current Run = ',RUN

do i1=1,N1
   NofV(i1)=0
enddo

E = RUN - 1
N=M
open(1,file="warray.txt")

do i1=1,N                    !generating  Poisson initial condition
   counter = 0
   do while(PR > exp(-lambda))
      PR=PR*DUNI()
      counter = counter +1
   enddo
   if (counter - 1 /= 0) then
      PV = counter - 1
   endif
```

```
   PR=1
   WX(i1)=PV
   write(1,*),WX(i1)
enddo

!do i1=1,N                    !generating uniform initial condition
!VL=27.0*DUNI()
!UV=Ceiling(VL)
!WX(i1)=UV
!write(1,*),WX(i1)
!end do

!print*,WX
!print*,'*******'

do
read(1,*,iostat=EoF)WX
if(EoF<0)exit
enddo

open(2,file="array.txt")
N=M
do i2=1,N
```

```
X(i2)=WX(i2)
write(2,*),X(i2)
enddo

time=0.0

!Time advancing starts here
 number = 0

do while(time <= tMax )
!print*,time

istat=.False.
jstat=.False.

T=0.0
S=0.0
A=0.0
B=0.0
Z_0=0.0

do i2=1,N-1
Z(i2)=0.0
```

```
enddo

do i3=1,N
F(i3)=0.0
end do

open(2,file="array.txt")
do
read(2,*,iostat=EoF)X
if(EoF<0)exit
enddo

open(4,file="radius.txt")
do i3=1,N
F(i3)=((3*X(i3))/(4*Pi))**(1.0/3.0)*(10)**(-5.0/3.0)
write(4,*)F(i3)
enddo

do read(4,*,iostat=EoF)F
if(EoF<0)exit
enddo

do k=1,N
```

```
  do l=1,N
    C(k,l)=0.0
  enddo
enddo

do k=1,N
  do l=k+1,N
    C(k,l)=((4*Pi)/(M))*((F(k)+F(l))**2)/(F(k)*F(l))
  enddo
enddo

open(3,file="vector.txt")
do k=1,N-1
  do l=k+1,N
    Z(k)=Z(k)+C(k,l)
    enddo
write(3,*)Z(k)
enddo

do
read(3,*,iostat=EoF)Z
if(EoF<0)exit
enddo
```

```
do k=1,N-1
Z_0=Z_0+Z(k)
enddo
!print*,Z_0

r_1=DUNI()
tau=(1/Z_0)*log(1/r_1)
!print*,tau

!generating i
do while(istat==.False.)
r_2=DUNI()
do p=1,N-1
T=T+Z(p)
if(T>=r_2*Z_0)then
i=p     !checking the first condition
exit
end if
enddo !print*,r_2

do q=1,i-1
S=S+Z(q)
```

```
enddo

if(S<r_2*Z_0)then        !checking the second condition
istat=.True.
end if

enddo

!generating j
do while(jstat==.False.)
r_3=DUNI()
do p=i+1,N
A=A+C(i,p)
if(A>=r_3*Z(i))then      !checking the first condition
j=p
exit
end if
enddo
!print*,r_3

do q=i+1,j-1
B=B+C(i,q)
enddo
```

```
if(B<r_3*Z(i))then      !checking the second condition
jstat=.True.
end if

enddo
!print*,i,j

do
read(2,*,iostat=EoF)X
if(EoF<0) exit
enddo

X(i)=X(i)+X(j)
do k=j,N-1
Aux=X(k)
X(k)=X(k+1)
X(k+1)=Aux
enddo

!collison counter starts here number=number+1

if(M-number==0) then
```

```
exit
endif

N=M-number

!The idea here is to remove old file array.txt and rewrite it with a
new, updated X array

close(2,status="Delete")

open(2,file="array.txt")
do i2=1,N
write(2,*)X(i2)
enddo

!print*,N

close(3,status="Delete")
close(4,status="Delete")
close(6,status="Delete")

time = time + tau
```

```
enddo  !time advancing

do i1=1, N1
   do j1= 1, N
      if(X(j1)==i1)then
         NofV(i1)=NofV(i1)+1
       endif
   enddo
enddo

do i1=1, N1
   N_av(i1)=(1.0/(E+1.0))*(E*N_av(i1) + NofV(i1))
enddo

do i1=1, N1
   Momnt(i1)= (1.0/(E+1.0))*(E*Momnt(i1) + NofV(i1)*NofV(i1))
enddo

close(1,status="Delete")
close(2,status="Delete")

enddo !run advancing
```

```
do i1=1,N1
St_dev(i1)=(Momnt(i1)-N_av(i1)*N_av(i1))**(1.0)/(2.0)
enddo

open(7,file="Naverage_100dr_1000r_01P.txt")
do i2=1,N1
   write(7,*),N_av(i2)
enddo
close(7)

open(8,file="Moment.txt")
do i2=1,N1
   write(8,*),Momnt(i2)
enddo
close(8)

open(9,file="Fluctuations.txt")
do i2=1,N1
   write(9,*),St_dev(i2)
enddo
close(9)

end program algorithm
```

Chapter 4

The Kinetic Coalescence Model

Suppose that the droplet spectrum is characterized by $N(x,t)$ such that $N(x,t)dx$ is the average number of droplets at time t per unit volume with masses between x and $x+dx$. The total number of coalescences per unit time experienced by droplets within this size interval is $N(x,t)\int_0^\infty N(x',t)C(x,x')dx'$. This integration describes the average rate of removal of x-droplets due to their coalescences with other droplets. These coalescence events reduce the number of drops on the interval dx. But the number of droplets on dx is increased by coalescences between all pairs of drops whose masses sum to x. This rate of increase is given by $\frac{1}{2}\int_0^x N(x',t)N(x-x',t)C(x',x-x')dx'$. The factor $\frac{1}{2}$ is necessary to prevent any particular coalescence configuration from being counted twice. Taking into account both effects, we obtain the following equation for the time rate of change of the average number of x-droplets $N(x,t)$

$$\frac{\partial}{\partial t}N(x,t) = \frac{1}{2}\int_0^x N(x',t)N(x-x',t)C(x',x-x')dx'$$
$$- N(x,t)\int_0^\infty N(x',t)C(x,x')dx' \tag{4.1}$$

This equation is well known as the kinetic equation or stochastic coalescence equation. The solution of (4.1) is $N(x,t)$, the droplet spectrum at time t which evolves by coalescence from a given initial distribution $N(x,0)$. This solution corresponds to the average value of $N(x,t)$ over many realizations of the droplet growth process.

The kinetic equation (4.1) is also referred to as the kinetic equation in the continuous form. Its discrete form,

$$\frac{dN_i(t)}{dt} = \frac{1}{2}\sum_{j=1}^{i-1} N_j(t)N_{i-j}(t)C_{j,i-j} - \sum_{j=1}^{\infty} N_i(t)N_j(t)C_{i,j} \tag{4.2}$$

given by (2.24) in the first chapter, was derived from the stochastic coalescence model by Gillespie. Now we will show how the continuous form links to the discrete one. Let $a = x_0 < x_1 < \ldots < x_n = b$, $\Delta x_k = x_k - x_{k-1}$, $x_{k-1} \le \xi_k \le x_k$, $d = max\Delta x_k$. Then

$$\int_a^b f(x)dx = \lim_{d\to 0}\sum_{k=1}^{n} f(\xi_k)\Delta x_k = \lim_{n\to\infty}\frac{b-a}{n}\sum_{k=1}^{n} f(a+\frac{k}{n}(b-a)).$$

We can assume that all Δx_k are the same and equal to Δx. Then $\Delta x = \frac{b-a}{n}$ and

$$\int_a^b f(x)dx = \lim_{\Delta x\to 0}\Delta x\sum_{k=1}^{n} f(a+k\Delta x) = \lim_{\Delta x\to 0}\Delta x f(x_k).$$

So $\int_a^b f(x)dx \sim \sum_{k=1}^{n} f(x_k)\Delta x$. The continuous form of the kinetic equation (4.1) is

valid for some x and t. Evaluate (4.1) at $x = x_i$.

$$\begin{aligned}\frac{\partial}{\partial t}N(x_i,t) &= \frac{1}{2}\int_0^{x_i} N(x',t)N(x_i-x',t)C(x',x_i-x')dx' \\ &- N(x_i,t)\int_0^{\infty} N(x',t)C(x_i,x')dx' \qquad (4.3)\end{aligned}$$

The first integral in (4.3) possesses an approximation

$$\int_0^{x_i} N(x',t)N(x_i-x',t)C(x',x_i-x')dx' \sim \sum_{k=1}^{m-1} N(x_k,t)N(x_i-x_k,t)C(x_k,x_i-x_k)\Delta x.$$

The second one

$$\int_0^{\infty} N(x',t)C(x_i,x')dx' \sim \sum_{k=1}^{\infty} N(x_k,t)C(x_i,x_k)\Delta x.$$

Then (4.3) becomes

$$\begin{aligned}\frac{\partial}{\partial t}N(x_i,t) \sim \frac{1}{2}\sum_{k=1}^{m-1} N(x_k,t)N(x_i-x_k,t)C(x_k,x_i-x_k)\Delta x \\ -N(x_i,t)\sum_{k=1}^{\infty} N(x_k,t)C(x_i,x_k)\Delta x. \qquad (4.4)\end{aligned}$$

In both discrete and continuous forms of the kinetic equation $N(x,t)$ is an average or expected number of droplets of type x at time t, while $C(x,x')$, the coalescence function, has different meanings. In the discrete case $C(x_i,x_j) = C(i,j)$ is a probability for particles x_i and x_j to coalesce but in the continuum case $C(x,x')$ is the probability density of coalescence, so that $C(x,x')dx'$ is the probability for particle x to coalesce with a particle in the interval $(x', x'+dx')$. Hence let $C(x,x')dx' \sim C(x_i,x_k)\Delta x \sim C(i,k)$. So

$$N(x_k,t) \sim N(k,t), \;\; N(x_i-x_k,t) \sim N(i-k,t),$$

$$C(x_i, x_k)\Delta x \sim C(i,k), \;\; C(x_k, x_i - x_k)\Delta x \sim C(k, i-k).$$

After substitution these equivalents into (4.4) we obtain a discrete form of the kinetic equation.

In this chapter we solve the discrete form of the kinetic equation by Euler's and forth order Runge-Kutta methods [10]. As the coalescence function we take the kernel specific for the Brownian diffusion and as the initial data we use an ensemble obtained by averaging Poisson and uniform distribution sample realizations created in the Fortran implementation of the Gillespie's algorithm in Chapter 2. Euler's method is a simple one-step method to approximate the solution to the first order differential equation

$$y' = f(t, y)$$

Let $\Delta t = (t_f - t_0)/n$ be the step size, t_f, t_0 and n being the final time, initial time and the number of time intervals, respectively, the approximated solution w is sought at equally spaced intervals with

$$w_{i+1} = w_i + \Delta t f(t_i, w_i), \qquad w_0 = y_0, \qquad t_i = t_0 + i\Delta t \;\; (i = 0, 1, 2, \ldots, n)$$

The method is derived by expanding the exact solution in a Taylor series about the point $t = t_i$, producing

$$y(t) = y_i + (t - t_i)y_i' + \frac{1}{2}(t - t_i)^2 y''(\xi)$$

where ξ lies between t and t_i. Evaluating the above expansion at $t = t_i$ and substituting for y_i' with the right hand side of the differential equation, we obtain

$$y_{i+1} = y_i + \Delta t f(t_i, y_i) + \frac{1}{2}\Delta t^2 y''(\xi)$$

Euler's method arises by dropping the error term $\frac{1}{2}\Delta t^2 y''(\xi)$, which is the local discretization error, and replacing y_i by w_i. Euler's method is by far the simplest one-step method to implement, however it is also not very efficient and in particular its global error, i.e. the error between the exact and approximate solution at the final time is $O(\Delta t)$. Higher order one-step Taylor methods can be constructed using the derivatives of f of the appropriate order. These higher order derivatives are not always available, which makes higher order Taylor methods not very attractive to implement. Runge-Kutta methods provide an alternative as they use exclusively the values of f to obtain the approximation of the appropriate order. In the fourth order case, the most common scheme updates the approximate solution at each time step according to the formula

$$w_{i+1} = w_i + \frac{1}{6}(k_1 + 2k_2 + 2k_3 + k_4),$$

where

$$\begin{aligned} k_1 &= \Delta t f(t_i, w_i) \\ k_2 &= \Delta t f(t_i + \frac{\Delta t}{2}, w_i + \frac{k_1}{2}) \\ k_3 &= \Delta t f(t_i + \frac{\Delta t}{2}, w_i + \frac{k_2}{2}) \\ k_4 &= \Delta t f(t_i + \Delta t, w_i + k_3) \end{aligned}$$

The method requires four function evaluations per time step and is of $O(h^4)$.

We verified the convergence of both Euler and Runge-Kutta 4th order methods by analyzing their global discretization error. For any method of order p, the global discretization error $\|e\|$ is of the form

$$\|e\| = C\Delta t^p, \quad \text{where} \quad \|e\| = \|\text{exact solution - approximate solution}\| \tag{4.5}$$

Here $\|.\|$ is a norm; C is a constant. Taking logarithm of both sides, we can write equation (4.5) as

$$\ln \|e\| = \ln C + p \ln \Delta t$$

If we plot $\ln \|e\|$ as a function of $\ln \Delta t$, then in a loglog plot $\|e\|$ vs Δt should approximately have a slope of p.

Since the exact solution is not available, we first obtain a reference solution to the exact solution by using the smallest (in our computation) time-step of $\frac{0.01}{2^5}$. All other numerical solutions are obtained with larger time steps and compared with the "exact" (reference) solution. Any norm can be used, for example, the $\| \cdot \|_\infty$. We examine the norm of the error between the reference solution and the solution at various time steps of $\frac{0.01}{2^k}$, where $k = 0, 1, \ldots, 4$ using a loglog plot, and indeed we achieve linear convergence and quartic convergence for Euler's method and Runge-Kutta 4th order method, respectively (see Figures 4.1 and 4.2).

We see that the error for Runge-Kutta method converges to zero faster than the error for the Euler's method as the step size decreases to zero. In particular, as the time step decreases by half, the error in Euler's method also decreases approximately by half and the error in Runge-Kutta method decreases by 1/16, which demonstrates the linear and 4th order convergence.

Since in Runge-Kutta method the coefficients k_1, k_2, k_3, k_4 need to be evaluated on every time step and the function f contains two sums, it would be more time efficient to apply Adams-Bashforth four step method instead. It is defined by equations

$$w_0 = \alpha, \quad w_1 = \alpha_1, \quad w_2 = \alpha_2, \quad w_3 = \alpha_3,$$

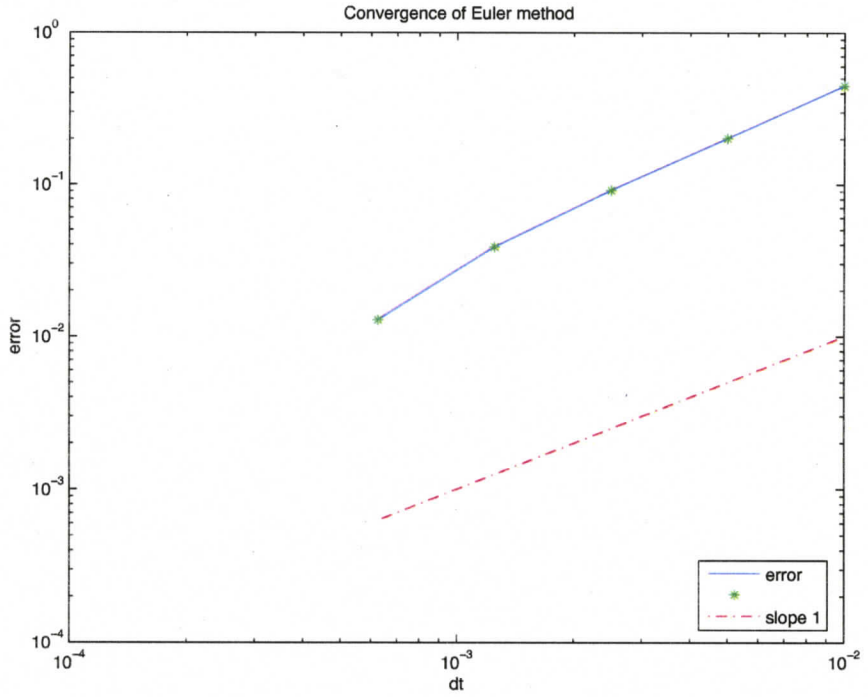

Figure 4.1: Convergence of Euler's method.

$$w_{i+1} = w_i + \frac{h}{24}(55f(t_i, w_i) - 59f(t_{i-1}, w_{i-1}) + 37f(t_{i-2}, w_{i-2}) - 9f(t_{i-3}, w_{i-3})).$$

This method uses an information from four previous steps and to get it started a one-step method of the same accuracy, such as Runge-Kutta of order four, for instance, needs to be applied until values w_1, w_2 and w_3 are computed. This method is of order $O(\Delta^4)$.

The kinetic equation in the continuous form (4.1) can also be solved numerically. In this case, we would need to discretize the right hand side of (4.1), i.e. evaluate the integrals of the type $\int_a^b f(x)dx$

$$\int_a^b f(x)dx \sim \sum_{i=1}^{M} c_i f(x_i)$$

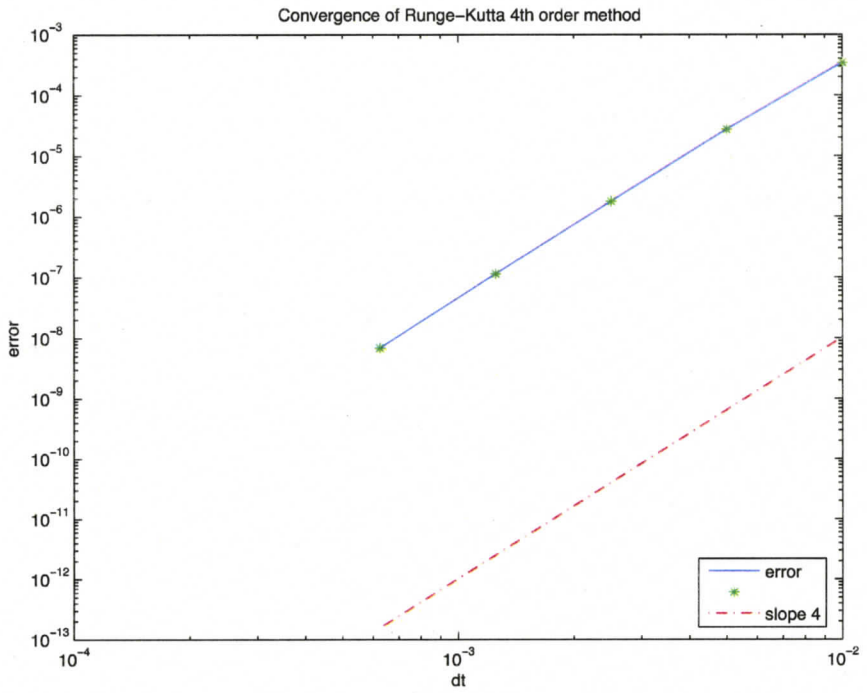

Figure 4.2: Convergence of Runge-Kutta 4th method.

where c_i are some weight coefficients. Mesh points x_i are usually chosen to be equispaced but this is not necessary.

Various methods can be employed, among them are Trapezoidal and Simpson's rules. Both result from approximating the integrand f on the interval $[a, b]$ by a piecewise polynomial function, piecewise linear and piecewise quadratic respectively, and then integrating the piecewise polynomial to obtain an approximation to the integral.

Suppose that the interval $[a, b]$ is subdivided into M subintervals $[x_k, x_{k+1}]$ of width $\Delta x = (b-a)/M$ by using the equally spaced nodes $x_k = a+k\Delta x$, for $k = 0, 1, \ldots, M$. The Composite Trapezoidal rule for M subintervals can be expressed in any of three

equivalent ways:

$$T(f, \Delta x) = \frac{\Delta x}{2} \sum_{k=1}^{M} (f(x_{k-1}) + f(x_k))$$

or

$$T(f, \Delta x) = \frac{\Delta x}{2}(f_0 + 2f_1 + 2f_2 + 2f_3 + \ldots + 2f_{M-2} + 2f_{M-1} + f_M)$$

or

$$T(f, \Delta x) = \frac{\Delta x}{2}(f(a) + f(b)) + \Delta x \sum_{k=1}^{M-1} f(x_k).$$

The global discretization error for this method [10] is

$$E_T(f, \Delta x) = \frac{-(b-a)f^{(2)}(\xi)\Delta x^2}{12}$$

where ξ is some constant between a and b. In other words, Trapezoidal rule is 2nd order accurate.

For the Composite Simpson's rule the integer M has to be even and this method can be expressed in any of three equivalent ways:

$$S(f, \Delta x) = \frac{\Delta x}{3} \sum_{k=1}^{M} (f(x_{2k-2}) + 4f(x_{2-1k}) + f(x_{2k}))$$

or

$$S(f, \Delta x) = \frac{\Delta x}{3}(f_0 + 4f_1 + 2f_2 + 4f_3 + \ldots + 2f_{2M-2} + 4f_{2M-1} + f_{2M})$$

or

$$S(f, \Delta x) = \frac{\Delta x}{3}(f(a) + f(b)) + \frac{2\Delta x}{3} \sum_{k=1}^{M-1} f(x_{2k}) + \frac{4\Delta x}{3} \sum_{k=1}^{M} f(x_{2k-1}).$$

It's global error is

$$E_S(f, \Delta x) = \frac{-(b-a)f^{(4)}(\xi)\Delta x^4}{180}$$

i.e. Simpson's method is 4th order accurate. Note that one can use the global discretization error to estimate the number of subintervals required to get a specified accuracy.

Both Trapezoidal and Simpson's rules belong to the class of Newton-Cotes formulas. Their main property is they have the fixed accuracy and error will decrease if Δx decreases provided that the second and fourth order derivatives of $f(x)$ are bounded for Trapezoid and Simpson's methods, respectively.

Another class of integration formulas consists of so called Gauss quadratures. The mesh points x_i, $i = 1, \ldots, M$ are usually not equispaced and are chosen to minimize the error between function f and its interpolating polynomial. These mesh points are roots of Legendre polynomials and they are located on $(-1, 1)$. If other interval $[a, b]$ is given, a simple translation formula can reduce $[a, b]$ to $[-1, 1]$. The weight coefficients c_i need to be computed as well. Both roots of Legendre polynomials and weights in Gauss quadratures have to be tabulated before integration formulas can be used. This complicates the use of these methods although they are much more accurate than Newton-Cotes formulas. For example, the 3-point Gauss quadrature rule is

$$\int_{-1}^{1} f(x)dx \sim \frac{5}{9} f\left(-\sqrt{\frac{3}{5}}\right) + \frac{8}{9} f(0) + \frac{5}{9} f\left(\sqrt{\frac{3}{5}}\right)$$

with the error

$$E_3 f = \frac{f^{(6)}(\xi)}{15,750}$$

Note that the error is very small and does not depend on Δx. It only depends on the smoothness of the function $f(x)$.

Chapter 5

Stochastic Versus Kinetic Model: Numerical Results

In this chapter we compare numerical solutions obtained by the methods described in Chapters 3 and 4. As initial conditions, we use uniform and Poisson distributions. First, we analyze whether full stochastic and kinetic models give comparable solutions at early times. Then we look at the long time evolution. We also investigate the effect of the number of points used in simulations. Lastly, we study the growth of a single large particle as it falls through smaller ones.

5.1 Complete Stochastic Particle Model

First we implement Gillespie's algorithm [24] for numerically simulating the stochastic coalescence process in a cloud with initial conditions sampled from both uniform and Poisson distributions. As an example of a mechanism for relative motion of particles

we consider Brownian motion taking 100 droplets in a unit volume with concentration 1%. The results are computed in terms of t_b, a characteristic time, defined by the time scale necessary to nondimensionalize the equations for the coalescence kernel. If t is our actual time variable, then we set

$$t = \alpha * t_b$$

with α, a nondimensionalized time, is our new variable. We consider two final integration times corresponding to α: 0.05 and 0.1. The characteristic time t_b is derived by I.A.Valioulis and E.J.List in [60]. We set t_b equal to 1 by rescaling the collision function $C(i,j)$ for Brownian motion, thus making the final time to be 0.05 and 0.1. The function $C(i,j)$ for Brownian motion is [60]

$$C(i,j) = \frac{2kT}{3\nu}\frac{(r_i + r_j)^2}{r_i * r_j},$$

where k is the Boltzmann constant, T is an absolute temperature and ν is a kinematic viscosity of fluid. After rescaling it takes the following form

$$C(i,j) = \frac{4\pi}{100}\frac{(r_i + r_j)^2}{r_i * r_j},$$

where r_i, r_j are the radii of the corresponding droplets i and j. To get statistically complete results, we carry out 1000 independent realizations each starting from the specific initial distribution drawn from Poisson and uniform distributions and proceeding to the same final time t. To simulate a Poisson random variable with mean λ, we generate independent uniform $(0,1)$ random variables $U_1, U_2, \ldots$ stopping at

$$N + 1 = \min\{n : \prod_{i=1}^{n} U_i < \exp^{-\lambda}\}.$$

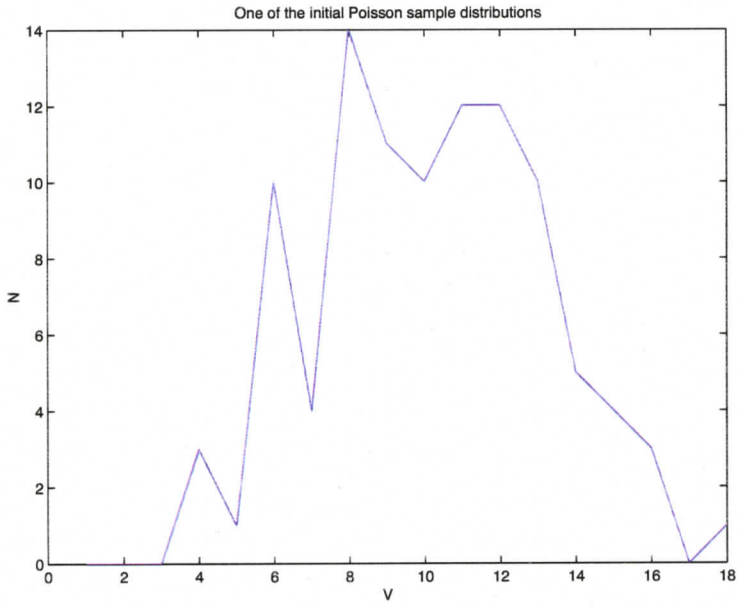

Figure 5.1: One of the initial Poisson sample distributions

Then $Prob\{X = N\} = \frac{\lambda^N}{N!}$ [49]. The figure 5.1 shows one of the initial Poisson sample distributions.

To generate a uniform distribution initial data we use the output values of a uniform random number generator to create the values of volumes from 1 to 27 where 27 is the maximum volume generated in Poisson initial distribution. The figure 5.2 shows one of the initial uniform distributions.

Figures 5.3 (a) and (b) show average concentration N of droplets using uniform distribution initial data for the two different final times $t_b = 0.05$ and $t_b = 0.1$ with numerical estimates of the fluctuations above the average in the droplet size spectrums. Δ of the graphs is the standard deviation. We observe that the maximum concentration average $N \approx 1.2$ is achieved at volume $v = 30$ for $t = 0.05$. We can

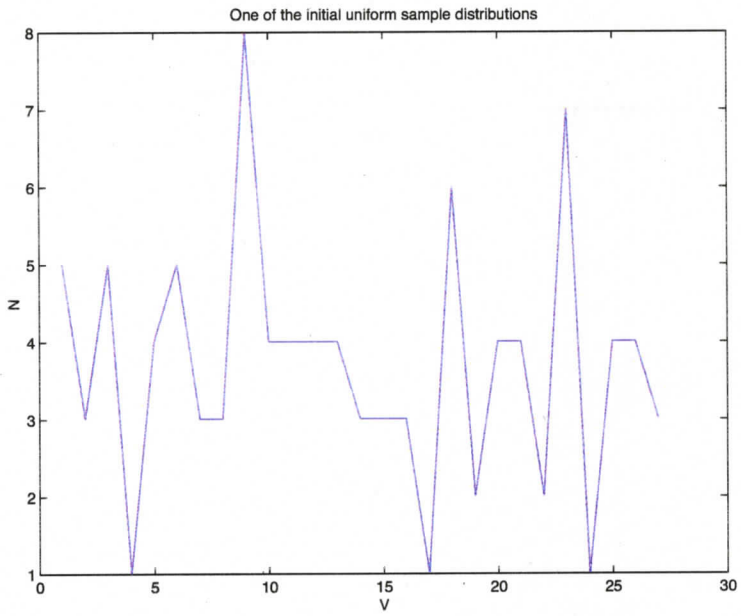

Figure 5.2: One of the initial uniform sample distributions

notice that as volume increases, the average concentration also increases with some fluctuations until it reached its maximum value but then it sharply drops by about a half of its maximum value and then it goes to zero also with small fluctuations. This sharp jump can be easily explained by the facts that initially we have no droplets larger in size than 27 and that the Brownian motion favors the coalescence of small droplets. The width of the spectrum is about 150. As final time increases to $t = 0.1$, i.e. twice, the maximum average concentration decreases by about twice but it still occurs at $v = 30$. A similar but weaker sharp jump to the right from the maximum value of the average concentration is observed. The width of the spectrum increases to about 250.

Next two figures 5.4 (a) and (b) show the average concentration at the same final

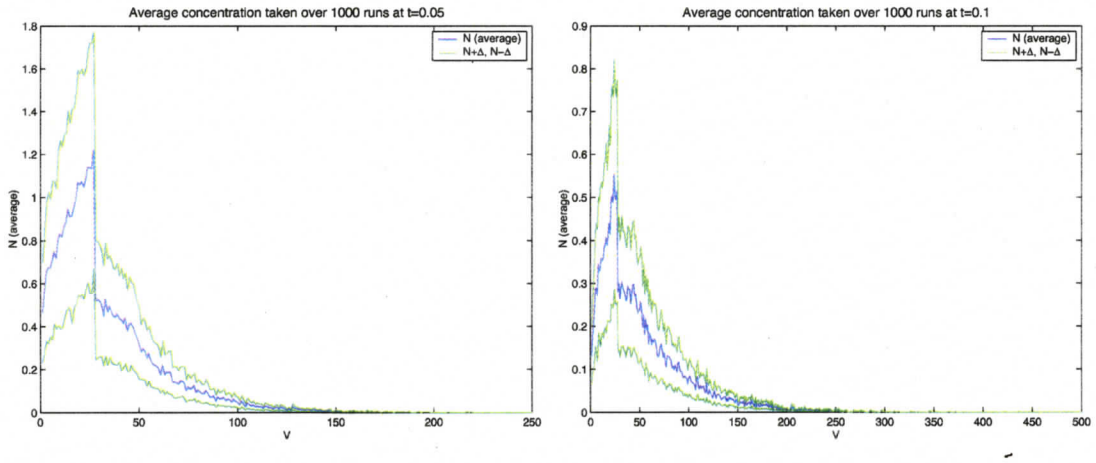

Figure 5.3: Full stochastic model: average concentration of droplets using initial Uniform distribution taken over 1000 runs at time (a) $t = 0.05$; (b) $t = 0.1$.

times but for Poisson distribution. There are several major differences between results for Poisson and uniform distributions. First, the average concentration for Poisson initial condition increases monotonically until the maximum point, i.e. without fluctuations unlike for the uniform initial data. The value of the maximum for Poisson distribution at the same final time is about twice more than for the uniform initial condition. After the maximum point, as volume increases, the average concentration with Poisson initial condition decreases again monotonically until it reaches about the half of the maximum value. Then average concentration fluctuates and goes to zero in a similar fashion as with uniform initial conditions. The spectrum for Poisson initial data is more narrow than for uniform initial data. Its width is about 100 and 150 for final times 0.05 and 0.1, so the spectrum width also increases as the final time increases but it is somewhat smaller than for the uniform initial data, case in Fig.5.3.

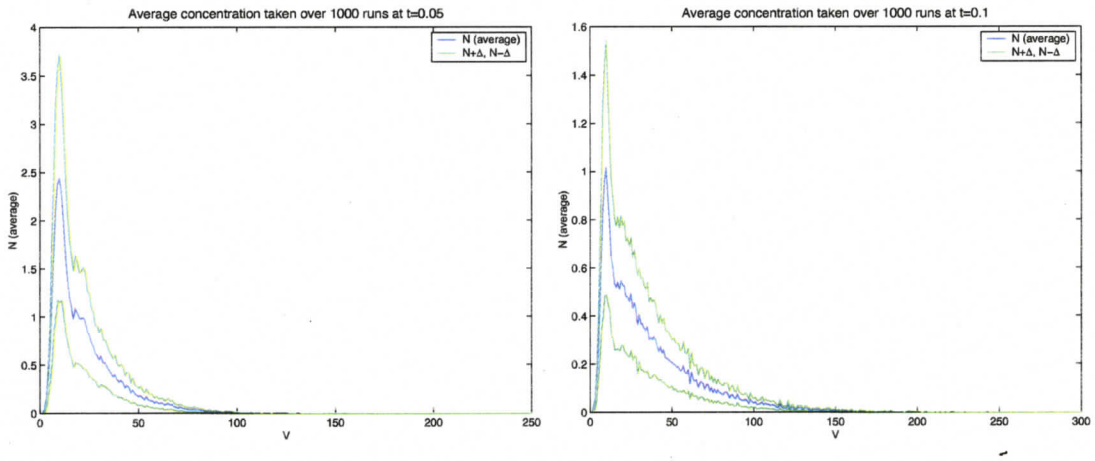

Figure 5.4: Full stochastic model: average concentration of droplets using initial Poisson distribution taken over 1000 runs at time (a) $t = 0.05$; (b) $t = 0.1$.

5.2 Kinetic Model

In this section we solve the initial value problem for the kinetic equation (4.2) by using the Runge-Kutta 4th order method described in Chapter 3. As initial droplet size spectrums we take the ensemble averages over 1000 for both the Poisson and uniform distribution sample-realizations. The next two figures show the graphs of these averages.

Solutions are computed at the same final times 0.05 and 0.1 with the time step $\Delta t = 0.001$. Since the kinetic coalescence equation is an approximation of the complete stochastic coalescence model, solutions will in principle approach each other as the number of droplets increases. A solution to the kinetic equation, i.e. the average concentration, will not have fluctuations unlike a solution to the complete stochastic model as some correlations in the derivation of the kinetic equation were assumed to be absent. Moreover, we can only compute numerically the average concentration N

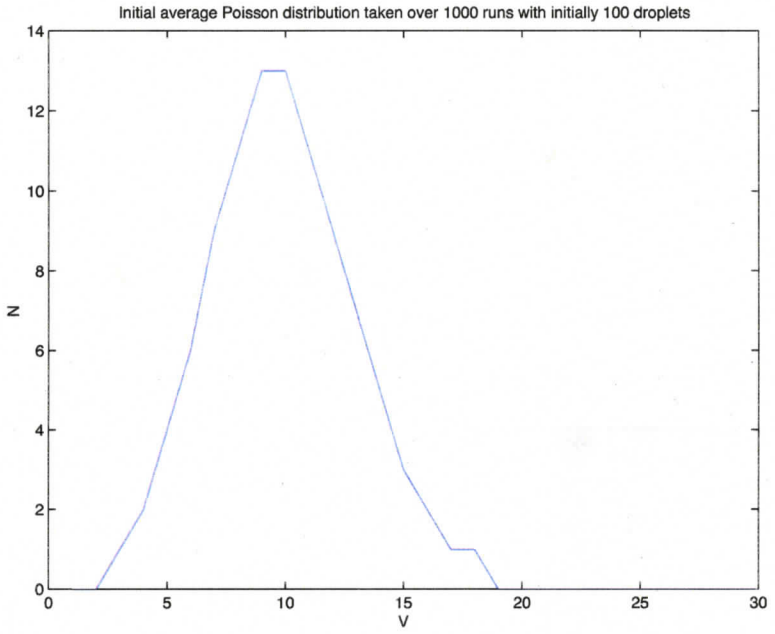

Figure 5.5: An average initial Poisson distribution taken over 1000 runs with initial 100 droplets

and not the standard deviation Δ.

The graphs in Figs. 5.7 (a), (b) show the average concentration from initial uniform distribution at $t = 0.05$ and $t = 0.1$. In the first figure, the maximum of the average concentration is slightly above 1.2 and it occurs at $v = 30$. This is in agreement with the results from the complete stochastic coalescence model. We also observe a sharp jump to the right from the maximum point and this jump is about the half of the maximum value as for the complete model. Then as volume increases concentration decreases to zero. What is different from the complete model is the behavior of the average concentration for small droplet volumes. In the case of the kinetic model, it increases sharply from zero to the value 0.6 which is the

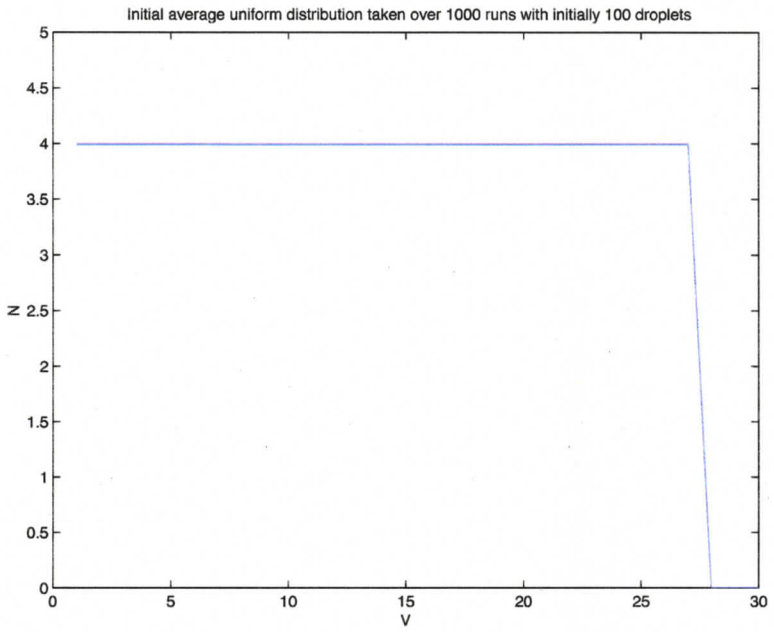

Figure 5.6: An average initial uniform distribution taken over 1000 runs with initial 100 droplets

half of the maximum concentration over the volume range and then increases to its maximum value much more slowly. The growth rate in the case of the complete stochastic model does not have this sharp change but we should notice that average concentration starts from 0.5 in this case. Then for small but not very small volumes we have an agreement between both solutions if small fluctuations are neglected in the complete stochastic model.

As the final time increases from 0.05 to 0.1, the maximum concentration decreases by half. The volume size at which the maximum occurs does not change. The width of the spectrum increases. This is again in qualitative agreement with the results from the complete stochastic model.

Figures 5.8 (a) and (b) present solutions of the kinetic equation from Poisson

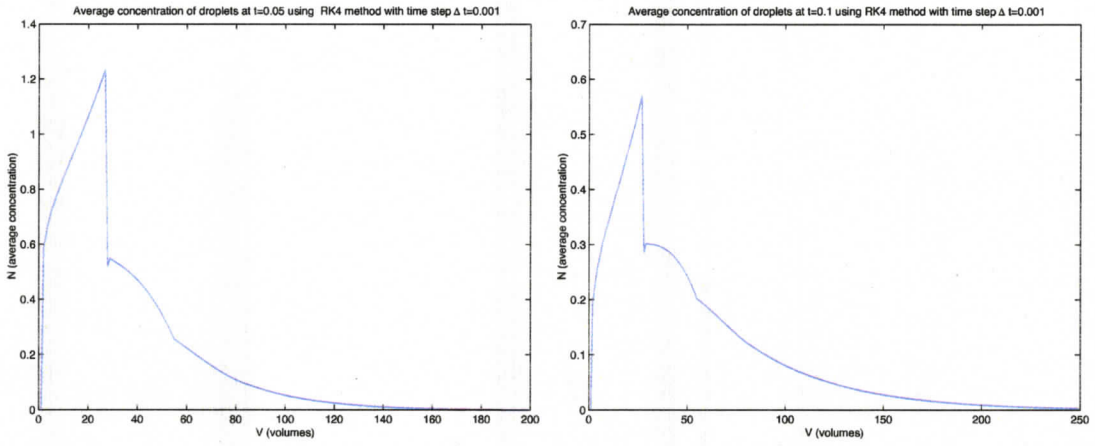

Figure 5.7: Kinetic model: average concentration of droplets using initial uniform distribution at time (a) $t = 0.05$; (b) $t = 0.1$.

initial distribution at final times 0.05 and 0.1. The maximum average concentration N at $t = 0.05$ is about 2.6 which is a bit higher than for the complete stochastic model where the maximum is about 2.4. Again we have monotonic growth of the average concentration in both models until the maximum value. Then concentration drops with a kink at about the half of the maximum value. After this kink, the decay rate decreases. The width of the spectrum is 100 which is approximately the same as for the complete model. At the later time 0.1, the maximum average concentration N decreases to its value 1.1, which is a bit greater than the solution of the complete model where maximum of N is about 1. We also observe big monotonic growth and decay rates before and after the maximum point, respectively. After that the concentration fluctuates at about 0.6 which is a half of the maximum N value and then the growth rate decreases and the concentration decays finally to zero. The spectrum width also broadens as for the complete coalescence model.

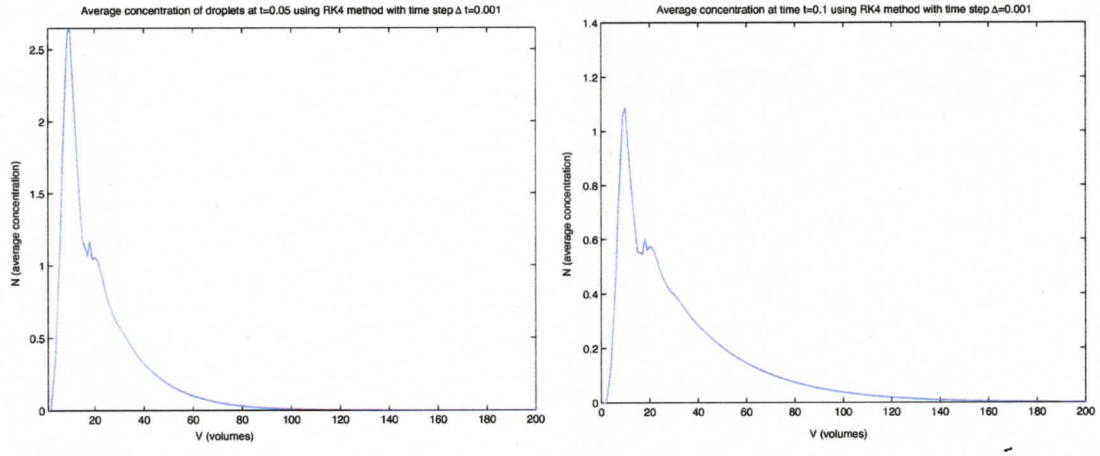

Figure 5.8: Kinetic model: average concentration of droplets using initial Poisson distribution at time (a) $t = 0.05$; (b) 0.1 .

We can conclude by saying that numerical solutions obtained by the full stochastic and kinetic models agree well at least for early times $t = 0.05$ and $t = 0.1$

5.3 Do Stochastic and Kinetic Models Agree?

In this section we continue comparing the full stochastic and kinetic models. In the previous section, we showed that these models are equivalent at least for early times $t = 0.05$ and $t = 0.1$. We would like to answer the following questions:

- Can long time evolution be studied by the stochastic and kinetic models? Do solutions agree?
- What is the effect of the number of droplets used in simulations?

We start by analyzing solutions obtained from Poisson and uniform initial distributions of 1000 droplets using both models. The average concentration $N(V)$ is

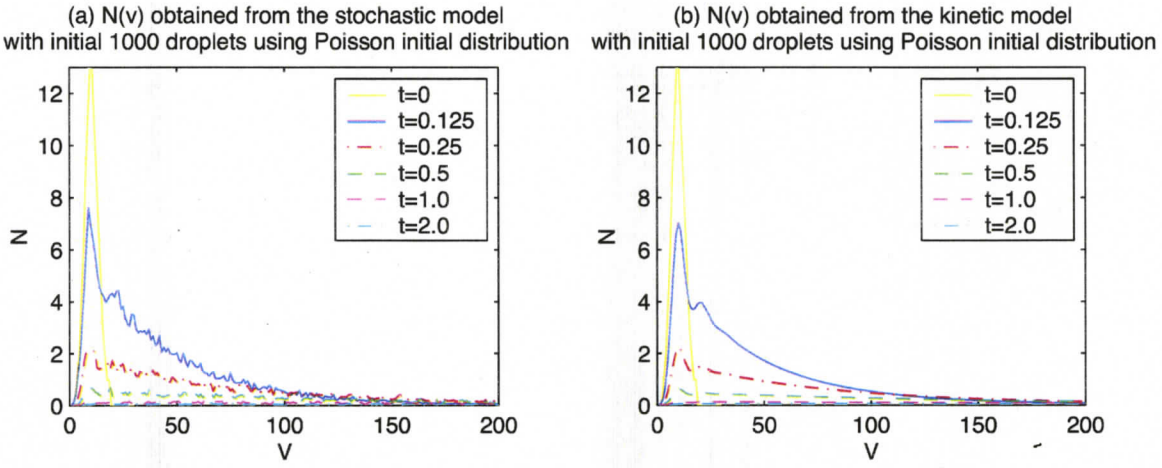

Figure 5.9: Average concentration $N(V)$ obtained at different times $t = 0.125$, 0.25, 0.5, 1.0 and 2.0 by (a) stochastic model with 1000 droplets at $t = 0$; (b) kinetic model.

computed at different times $t = 0.125$, 0.25, 0.5, 1.0 and 2.0 and plotted in Fig. 5.9 (a) and (b) for the case of stochastic and kinetic models, respectively . We observe that solutions agree quite well not only at early times but also at later times $t = 1.0$ and 2.0.

Next we study the effect of the number of particles used in numerical simulations. In the previous graphs we used 1000 droplets initially. Would we still have an agreement between the stochastic and kinetic models if we use fewer particles, say 100. In the next Figs. 5.11 and 5.12 we plot the average concentration $N(V)$ at $t = 0.05$, $t = 0.1$ and $t = 0.2$ obtained by the stochastic (a) and kinetic (b) models from Poisson and uniform initial distribution. As we can see, these models are still in a good agreement even for smaller number of points initially in the system. We should note that simulations are run only until $t = 0.2$. Due to the coalescence process, the number of particles in the stochastic model decreases and this poses the limitation on how long

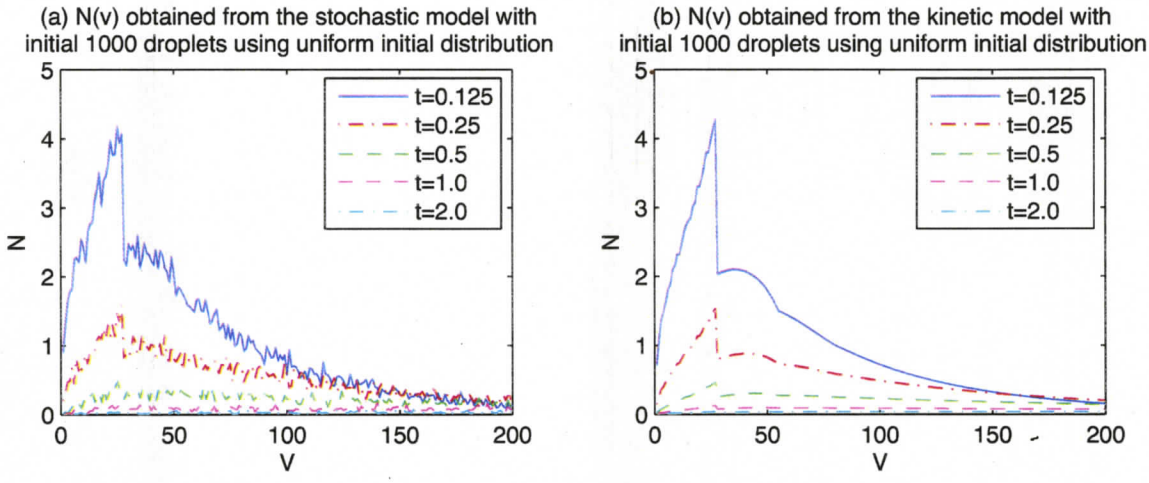

Figure 5.10: Average concentration $N(V)$ obtained at different times $t = 0.125$, 0.25, 0.5, 1.0 and 2.0 by (a) stochastic model with 1000 droplets at $t = 0$; (b) kinetic model.

we can run a program with a given number of points initially. Again, the stochastic models gives a little bit higher number of small droplets in the range $V < 30$ until the average concentration reaches a maximum at $V = 30$.

Therefore, starting with Poisson or uniform initial distributions of droplets, both the stochastic and the kinetic models agree not only for early but also for later times. These model give comparable solutions as in the case when there are a lot of droplets in the system initially but also when the number of droplets is not very high.

5.4 Large Droplet Evolution

The growth of a single particle as it falls through smaller ones has been a subject of many investigations. This problem is very important for atmospheric sciences since the rain formation in warm clouds is very sensitive to the growth rate of large

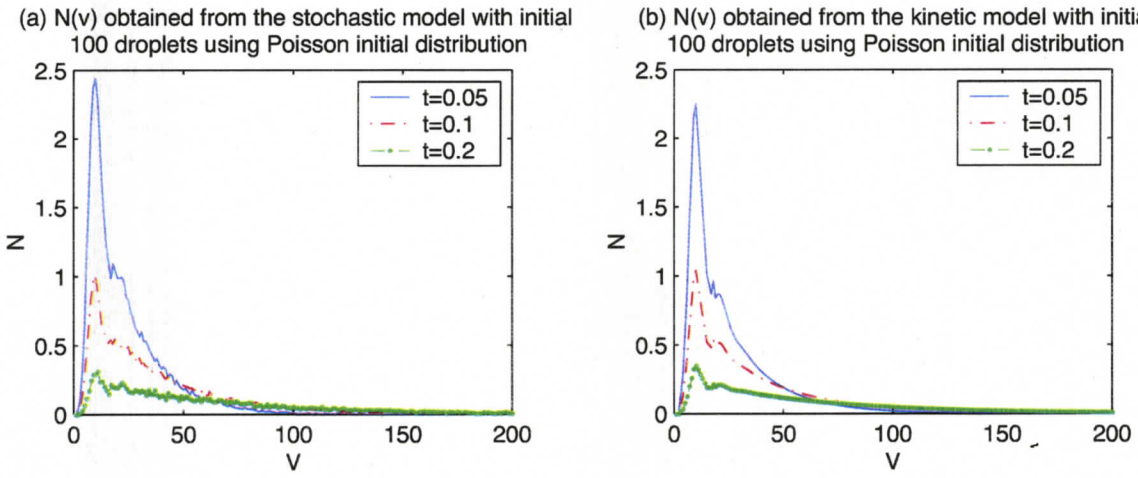

Figure 5.11: Average concentration $N(V)$ obtained at different times $t = 0.05$, $t = 0.1$, $t = 0.2$ by (a) stochastic model with 100 droplets at $t = 0$; (b) kinetic model.

particles. In this section we will analyze how fast a large droplet grows using both models.

We let a single particle, say of volume $V = 2$, settle through a monodisperse suspension of 200 particles of volume $V = 1$. Note that the volume of this single particle is twice any of the rest in a cloud. We then follow the growth of this large particle with the two models and compute the probability $P(V, t)$ of the large particle having a volume V at time t. The probability distributions obtained at three different times $t = 0.05$, 0.1 and 0.2 are shown in Figs. 5.13 (a) and 5.14 (a) using the stochastic and the kinetic models, respectively. We can clearly notice that even though probability density functions agree qualitatively, the stochastic model gives about twice less smaller particles and the largest droplet grows about twice faster than in the case of the kinetic model. This in fact demonstrates that the two models are not always equivalent. We should recall one of the assumptions under which the

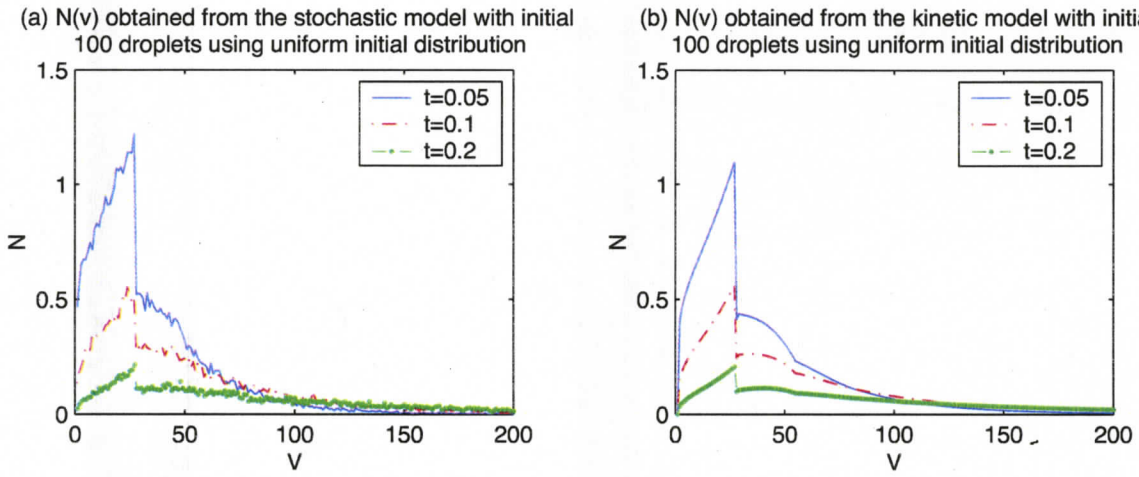

Figure 5.12: Average concentration $N(V)$ obtained at different times $t = 0.05$, $t = 0.1$, $t = 0.2$ by (a) stochastic model with 100 droplets at $t = 0$; (b) kinetic model.

kinetic model is derived by Gillespie, 1972 [23] is that the coalescence of particles of equal size is prohibited. In this problem, our initial condition is very special and all particles except of one, have the same volume. Therefore, it is expected that the two models should not agree in this case.

In order to evaluate the influence of the number concentration of the small particles on the probability density function $P(V, t)$ of the size of large particles, we repeat the calculations starting with an initial number of 100 elemental particles of volume $V = 1$ and one large droplet of the volume of two elemental particles, i.e. $V = 2$.

In this case, the stochastic model again predicts a faster growth rate (about 2 times faster) for the average size of the large particle.

These computations show different relations between the results of stochastic and kinetic models for the large droplet evolution than in the paper by Valioulis & List, 1984 [60] where the authors show that solutions agree well when 200 and 1 droplets

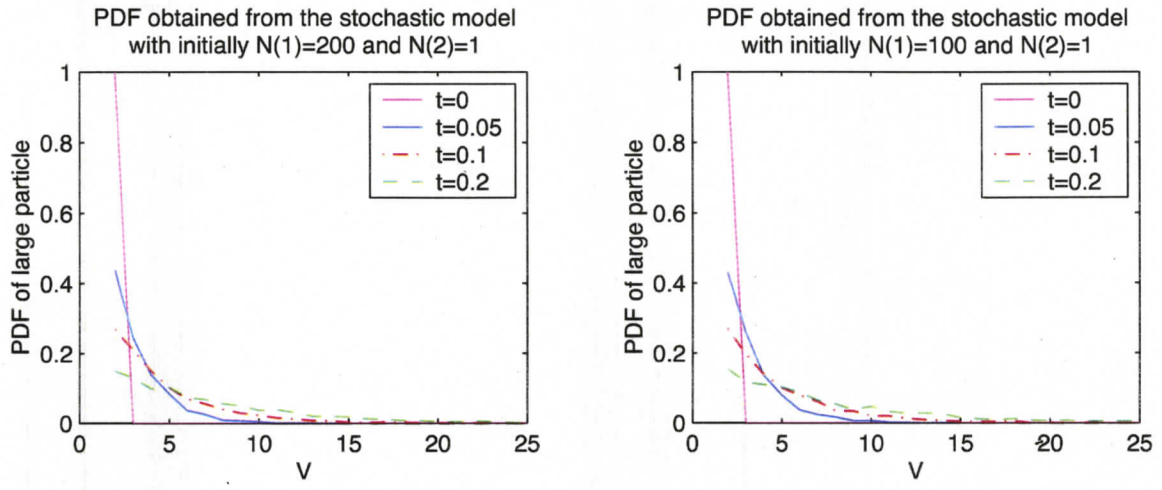

Figure 5.13: PDF for a large droplet evolution obtained using the stochastic model with initially (a) 200 droplets of volume 1 and one droplet of volume 2; (b) 100 droplets of volume 1 and one droplet of volume 2

are used at least for early time $t = 0.15$ and 0.3. They observe some disagreement at $t = 0.45$. When only 20 droplets are used in their simulations, the stochastic model predicts a faster growth rate for the average size of the large particle as in our cases done for 101 and 201 particles. We could not perform numerical simulations with 20 particles until our final time $t = 0.1$ and $t = 0.2$ as all particles completely aggregate much earlier.

Hence, the stochastic and the kinetic models do not give equivalent solutions when such special initial conditions are considered, namely when there are many particles of the same volume. This difference in solutions is justified in part by recalling the derivation of the kinetic equation from the stochastic model in section 2.3. The derivation requires that correlations between particles of the same size be neglected, i.e, $C(m, m) = 0$. Clearly, these numerical experiments, compared to the earlier

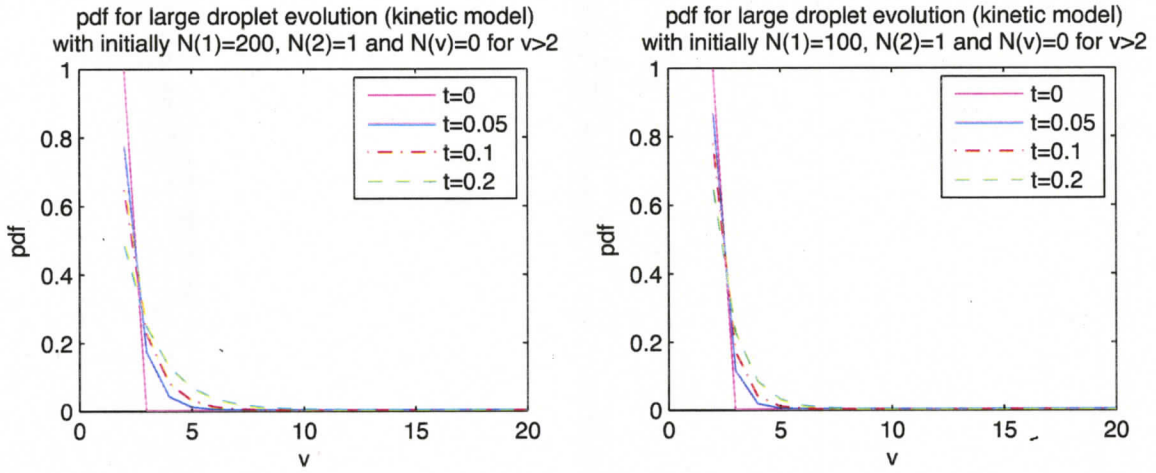

Figure 5.14: PDF for a large droplet evolution obtained using the kinetic model with initially (a) 200 droplets of volume 1 and one droplet of volume 2; (b) 100 droplets of volume 1 and one droplet of volume 2

runs where the two models agree with each other, demonstrate that correlations are important and cannot always be ignored. The difference with Valioulis & List results may be explained by different assumptions used in numerical simulations in this thesis and in the article. It is not clear from the article which process was considered (Brownian motion, laminar shear or differential sedimentation) whereas we use Brownian motion, moreover, we do not know if the authors placed any restriction on the coalescence of particles of the same size.

Chapter 6

Validation of Numerical Results by Comparison to Theoretical Predictions

6.1 Convergence to Poisson distribution

Here we validate the convergence result to Poisson distribution proved by Gillespie [23] and reported in Chapter 2. Namely, we are interested in the rate of convergence as $t \to \infty$ and as the number of droplets increases.

To study the convergence to Poisson distribution, we analyze the difference between mean μ and variance Δ^2 at different times. Since both mean and variance are vectors, we use their norms, specifically l_2 norm, to be able to compare results. We construct solutions at final times 0.25, 0.5, 1 and 2. Note that each successive time is twice bigger than the previous one in this final time sequence.

The top left graph in Fig. 6.1 (a) shows the dependence of the $\Delta^2 - \mu$ as a function of t. We clearly observe that the difference approaches zero as time t increases. At time $t = 0.25$ this difference is 1.328, while at $t = 2$ it decreases significantly to the value 0.048596. If the value of this difference was zero, we would have a true Poisson distribution since for this distribution the mean equals to the variance. In our case, we conclude that as the final time increases, the distribution of volumes does approach Poisson distribution

It is interesting to study how fast the difference between mean and variance goes to zero. Let us consider two models. In the first model, we assume that the difference $|\Delta^2 - \mu|$ decays exponentially, i.e.

$$|\Delta^2 - \mu| = C\,\mathrm{e}^{-\lambda t}$$

where C and λ are some constants. The equality has to be taken in the loose sense. For instance here we mean $|\Delta^2 - \mu| = O(\mathrm{e}^{-\lambda t})$. Taking logarithm of both sides we get

$$\ln|\Delta^2 - \mu| = \ln C - \lambda t$$

If the difference between mean and variance decays exponentially, then $\ln|\Delta^2 - \mu|$ would be a linear function of t, but as we see from Fig. 6.1 (b) (upper right), this is not the case as the curve is convex. Hence, we conclude that the $|\Delta^2 - \mu|$ does not decay exponentially.

Another model to consider is

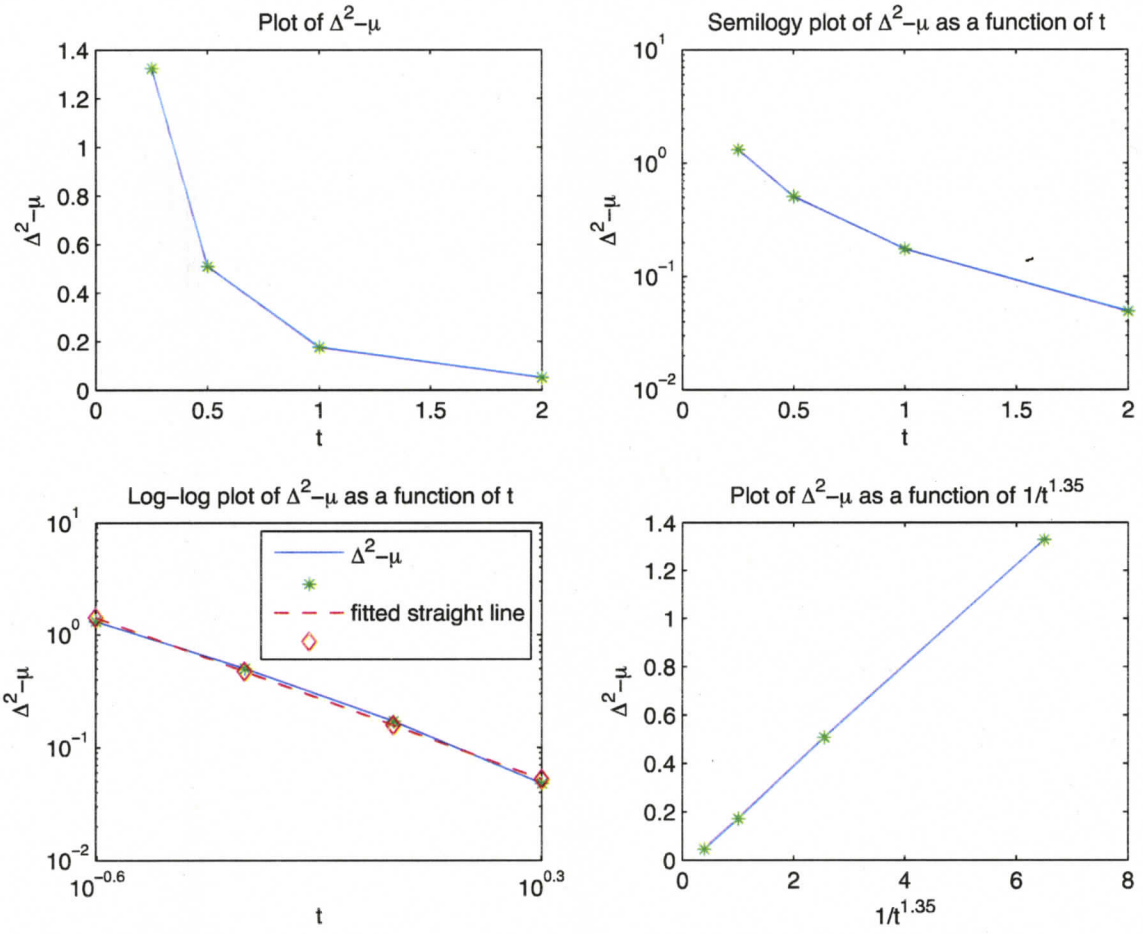

Figure 6.1: Study of the convergence to Poisson distribution: (a) $\Delta^2 - \mu$ as a function of t; (b) Log-linear plot of $\Delta^2 - \mu$ as a function of t (semilogy plot); (c) Log-log plot of $\Delta^2 - \mu$ as a function of t; (d) $\Delta^2 - \mu$ as a function of $1/t^{1.35}$

$$|\Delta^2 - \mu| = Ct^{-p}$$

i.e. the difference between mean and variance decays algebraically as some inverse power of t. Taking logarithm of both sides we get

$$\ln|\Delta^2 - \mu| = \ln C - p \ln t$$

i.e. $|\Delta^2 - \mu|$ is a linear function of $\ln t$. Looking at Fig. 6.1 (c) (left bottom) which is log-log plot of $|\Delta^2 - \mu|$ as a function of t, we see that the graph is close to the straight line with very small concavity. Using least square linear fitting we can compute the slope and y-intercept of this fitted straight line. Its equation is

$$\ln|\Delta^2 - \mu| = -1.5867 \ln t - 1.8408, \tag{6.1}$$

i.e. the slope is -1.5867. The better "graphical" fit is obtained by using the slope -1.35 as we can see from Fig. 6.1 (d) (right bottom). In other words, we assume that $|\Delta^2 - \mu|$ is proportional to $1/t^{1.35}$. Nevertheless, we will use results from linear least square fitting since we get both slope and free parameter. From equation (6.1) we obtain

$$|\Delta^2 - \mu| = \mathrm{e}^{-1.8408}\, t^{-1.5867}.$$

Using this relation we can compute, for example, given a tolerance ϵ, the difference

$$|\Delta^2 - \mu| < \epsilon$$

when time

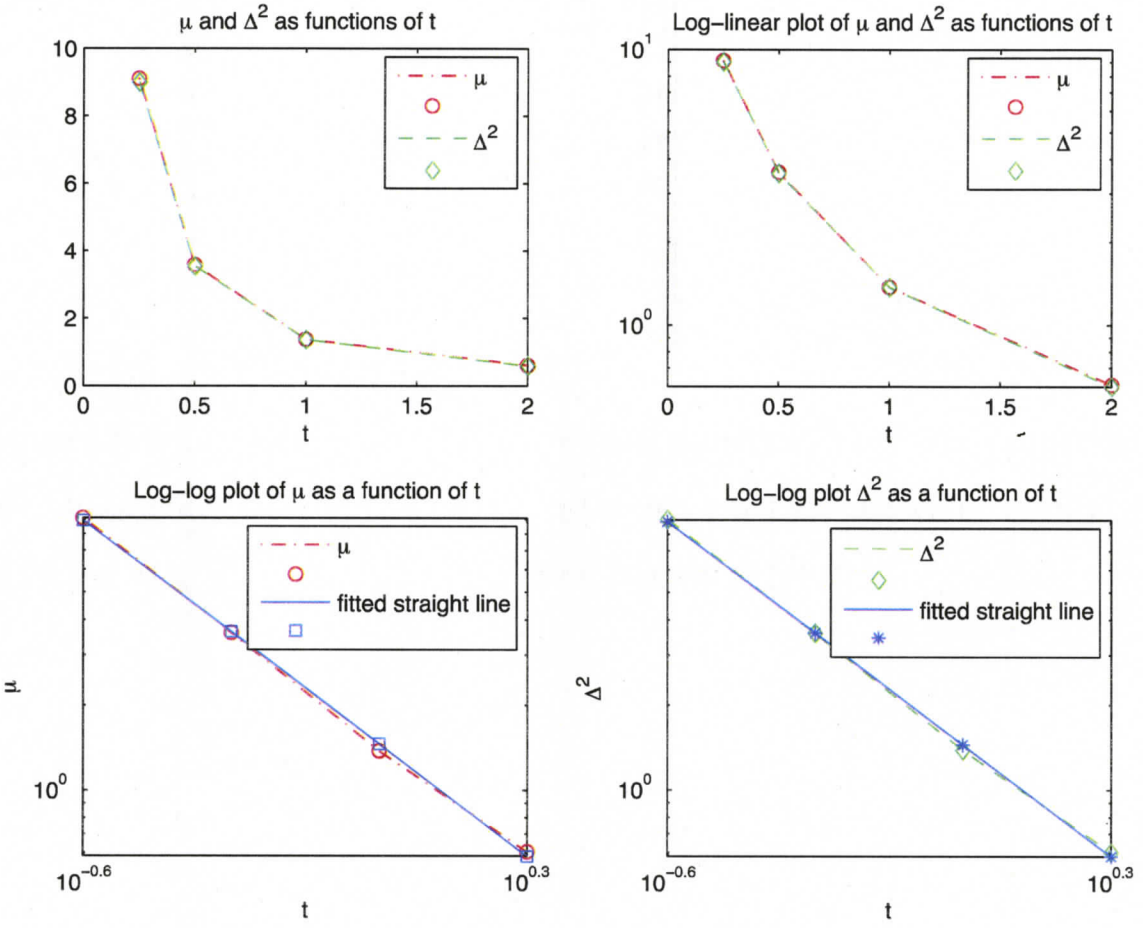

Figure 6.2: Analysis of norms of mean and variance as functions of t

$$t > \left(\frac{e^{-1.8408}}{\epsilon}\right)^{1.5867}$$

Another question to analyze is which value the norm of mean and variance approach to as t goes to infinity. In Fig. 6.2 (a) we plot both norms of mean μ and variance Δ^2 as functions of t. We observe that both norms decrease as time increases. Exponential decay of these functions is not possible since using log-linear plot of μ and Δ^2 as functions of t does not produce straight lines (see Fig. 6.2 (b)). Log-log

plots of μ and Δ^2 are shown in Fig. 6.2 (c) and (d), respectively. We observe that both graphs are very close to straight lines and we can conclude that norms of mean and variance decay as some inverse powers of t. Using linear least square fitting we obtain the following expressions:

$$\mu = \mathrm{e}^{0.3732}\, t^{-1.3092} \quad \text{and} \quad \Delta^2 = \mathrm{e}^{0.3654}\, t^{-1.3081}$$

The expressions for μ and Δ^2 are very close to each other. We should also notice that both μ and Δ^2 approach zero as $t \to \infty$. We then can conclude that as time increases, the solution becomes closer and closer to Poisson distribution with parameter, say, λ that also goes to zero as $t \to \infty$.

We can analyze pointwise convergence of the expected value, i.e. $N(V)$ and the variance $\Delta^2(V)$ as functions of V as time increases. In Figs. 6.3 (a) and (b) we plot the average concentration $N(V)$ of cloud droplets and their variance $\Delta^2(V)$ at times $t = 0.25$, 0.5, 1.0 and 2.0. Fig. 6.3 (c) contains their difference. We observe that for a volume V, both mean and variance tend to decrease as time increases. The reason for that is the coalescence process during which the number of droplets constantly decreases while large droplets are formed. Therefore, we expect the number $N(V)$ of large droplets to increase with time, although this is not very evident from the plots because of the stochastic noise. Recall the definition of the expected value $N(V)$ at time t as it is given in Gillespie, 1972 [23] .

$$N(V,t) = \sum_{n=0}^{\infty} n \cdot P(n,V,t), \tag{6.2}$$

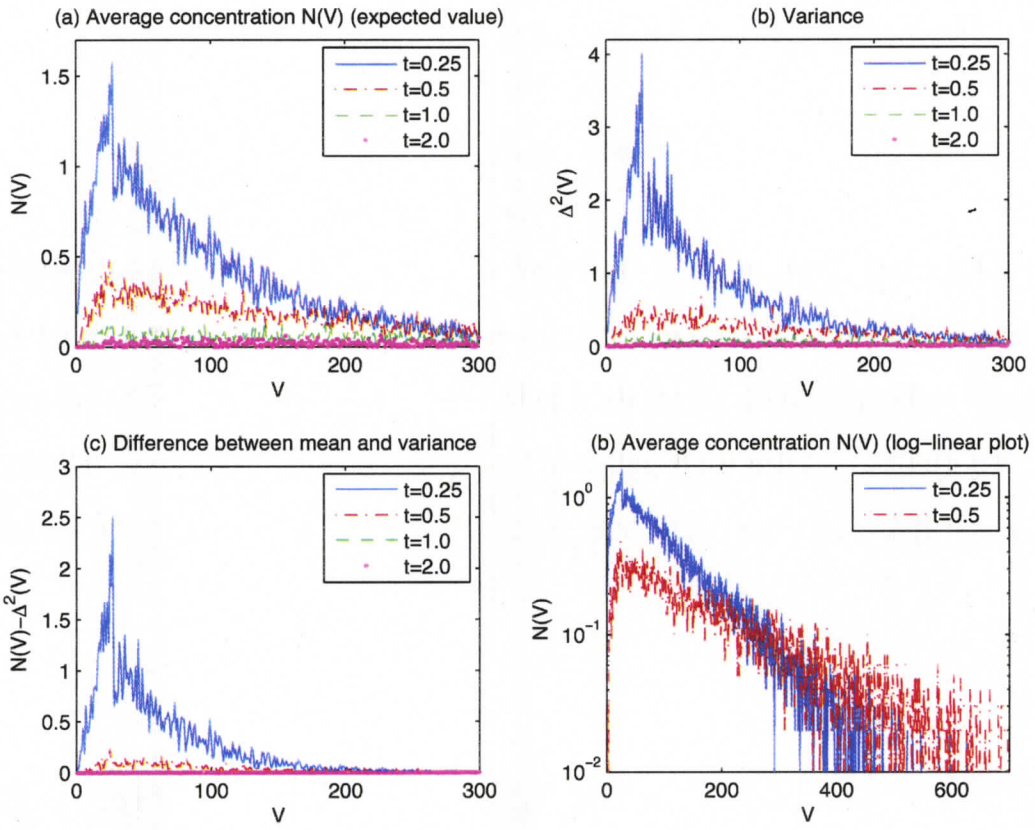

Figure 6.3: (a) Average concentration $N(V)$ (expected value) at times 0.25, 0.5, 1.0 and 2.0; (b) Variance; (c) Their difference; (d) $\ln N(V)$ as a function of V (log-linear plot)

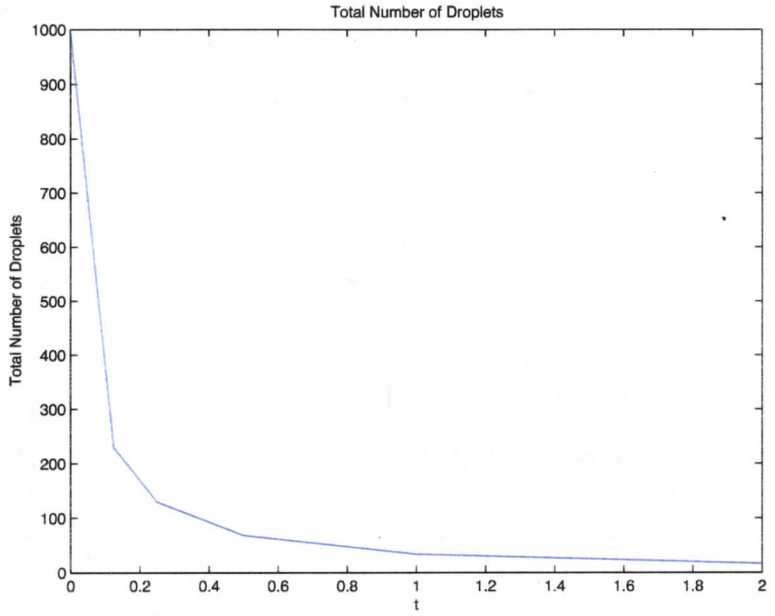

Figure 6.4: Total Number of Droplets in a Cloud

where

$$P(n,V,t) \equiv \text{probability that there are exactly } n \text{ droplets of volume } V \text{ in the cloud at time } t$$

Note that there are infinitely many terms in the sum in equation (6.2). In practice, we use only a finite number of droplets. More droplets we use, the more realistic approximation to cloud aggregation we have and more uniformly mixed the cloud is. However, the large number case is unpractical and therefore approximated by the continuous limit. So the infinite sum is replaced with

$$N(V,t) \approx \sum_{n=0}^{n_{max}} n \cdot P(n,V,t), \tag{6.3}$$

Because of the coalescence, the number of droplets decreases. Hence, n_{max} decreases with time. Since probabilities do not exceed the value one, we always have

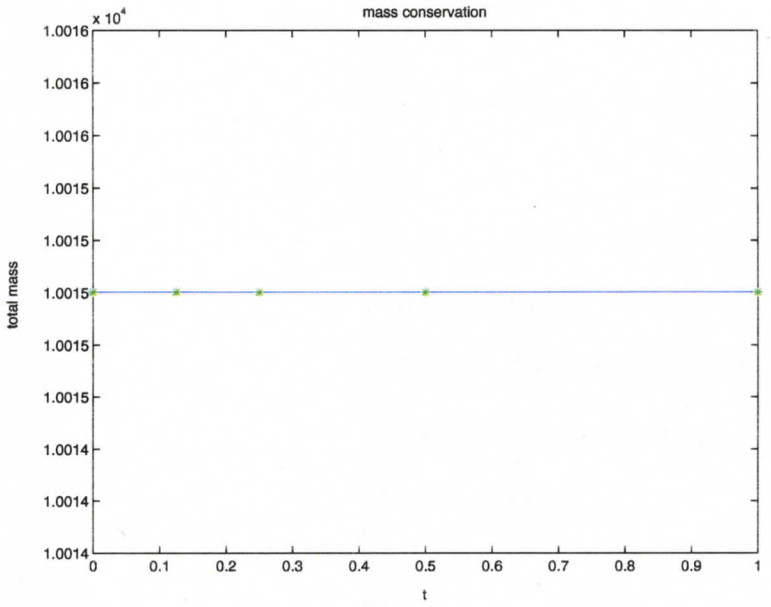

Figure 6.5: Total mass of droplets in a cloud as a function of time

an upper bound on the right hand side of (6.3), namely, n_{max}.

In particular, starting from 1000 particles distributed uniformly, at the end of each run we are left only with 230, 130, 69, 35 and 17 droplets at times 0.125, 0.25, 0.5, 1.0 and 2.0, respectively. We plot the total number of droplets as a function of t in Fig. 6.4. The plot in Fig. 6.5 shows the total mass in the system (actually, the total volume, we can assume that the density equals 1) by the formula

$$\text{Total Mass} = \sum_{V=1}^{V_{max}} V \cdot N(V)$$

We can conclude that the total mass is indeed conserved.

The decreasing number of particles is, in fact, one of the drawbacks of the direct stochastic simulation as was mentioned by Goodson and Kraft, 2004 [26]. The remedy to this problem is to either increase the number of droplets in a cloud, which will

reduce the efficiency of the algorithm, or to employ a technique which would add randomly created particles once some particle coalesce and the number of particles decreases. One of such techniques is called a *particle combining technique*, in which parallel arrays of particles are periodically combined to give an array with the desired number of particles (Sabelfeld et al., 1996 [50]). A natural extension of this technique is the *constant number simulation method* of Matsoukas and co-workers (Smith and Matsoukas, 1998 [55]; Lee and Matsoukas, 2000 [37]; Lin etal., 2002 [38]). Another approach to make the model more physically realistic is to add the effect of particle breakup as was considered by Telford et al., 1955 [57]. In this case, it is possible to obtain an equilibrium solution for N without decreasing concentration.

In reality we do not have a closed system as tiny droplets are constantly being formed due to evaporation from rising warm streams and consequent condensation. These droplets enter the system and the number of droplets in a cloud does not decrease critically. To incorporate this physical process, we would need to use one of the particle combining techniques mentioned above but this would complicate the problem and may be a subject of future investigation. The assumption of adiabatic cloud parcels is useful in cloud physics. In fact, the formation of cloud droplets occurs at cloud base (at high supersaturation) and the number of cloud droplets above cloud base does not increase with height. Rather conversion to rain droplets reduces the number of cloud drops.

We can make another observation from Figs. 6.3 (a) and (d) where the average concentration $N(V)$ and $\ln N(V)$ are plotted as functions of V at different times that as time increases, the mean $N(V)$ decreases for small volumes $V < 200$ and increases

for large volumes $V > 200$. For better presentation, Fig. 6.3 (d) contains results only for two times $t = 0.25$ and $t = 0.5$. The results for later times are very noisy. A less noisy result can be seen in Fig. 6.6 (a), (b) where the average concentration $N(V)$ and its logarithm are plotted at $t = 0.125$ and 0.25. Plot 6.6 (b) clearly indicates that the mean $N(V)$ for higher volumes, approximately $V > 150$ is smaller for earlier time.

6.2 The Marshall-Palmer Distribution of Raindrops with Size

From an empirical study of the distribution of rain droplets with size J.S. Marshall and W.M. Palmer, 1948 [42] concluded that such distribution could be adequately represented as negative exponential functions. Let $N(D)$ be a number of droplets of diameter D. Then for large droplets, $N(D)$ is approximately

$$N(D) = N_0 \cdot \exp(-\lambda D),$$

where N_0 is the value for $N(D)$ for $D = 0$. Marshall & Palmer found that the value N_0 was the same for any rain intensity R whereas the parameter λ was inverse proportional to some power of R.

We should note that our function N, obtained using the complete stochastic model developed by Gillespie, 1972 [23], depends on droplet's volume V and not on the diameter as in Marshall & Palmer's paper. In this section, we are interested in establishing whether the distribution of volumes or diameters/radii has Marshall-

Palmer distribution. In fact, we establish that the average concentration N as a function of volume V has exponential decay for large volumes as in the above equation. This is not a classical result as in Marshall-Palmer where diameters were used. When we consider N as a function of diameter D or radius r we still observe fast decay as diameters/radii increase because of one-to-one correspondence between volume, diameter and radius, but this decay is described by more complicated function than $\exp(-\lambda D)$ or $\exp(-\lambda r)$ as shown at the end of this section. The dependence of lambda on the rain intensity will not be a subject of our investigation.

We may work with the frequency distribution $N(V)$ as in Marshall & Palmer, 1948 [42] or we can study the relative frequency, i.e. probability of a droplet having volume V, i.e. $N(V)/N_{tot}$, where N_{tot} is the total number of droplets in a cloud. If the volumes of droplets have Marshall-Palmer distribution, then the probability can be written as

$$\frac{N(V)}{N_{tot}} = \lambda \, \mathrm{e}^{-\lambda V} \tag{6.4}$$

for an ideal situation when there is a continuous spectrum with an infinite number of droplets. Since we work with a discrete spectrum, we can approximate the relation (6.4) by $\frac{N(V)}{N_{tot}} = \tilde{\lambda} \, \mathrm{e}^{-\lambda V}$ where $\tilde{\lambda}$ approaches λ as the number of droplets increases.

In previous chapters, we used uniform and Poisson distributions of droplets as initial conditions. As a result, the average concentration $N(V)$ was obtained. We will investigate whether the distribution of volumes obtained from both initial distribution can be described by Marshall-Palmer distribution as time increases. Since the average concentration as a function of volume V first increases until it reaches its maximum and them decays to zero with the slower rate, the negative exponential function can

adequately describe $N(V)/N_{tot}$ only for large volumes, at least for those greater than the value at which the maximum of $N(V)$ is attained. We will analyze for which volumes the probability is in a better agreement with Marshall-Palmer distribution. We will also show that as time increases, λ and $\tilde{\lambda}$ approach each other approximately linearly in $1/t$, the same conclusion can be made about their difference.

First we will study the average concentration $N(V)$ obtained from the initial uniform distribution. If $N(V)$ has Marshall-Palmer distribution, then we can write

$$\frac{N(V)}{N_{tot}} = \tilde{\lambda}\, \mathrm{e}^{-\lambda V} \quad \text{for large } V \tag{6.5}$$

where parameters λ and $\tilde{\lambda}$ should approach each other as time increases. This would mean that the distribution of droplets becomes closer and closer to the Marshall-Palmer distribution. Taking logarithm of both sides of (6.5) we obtain

$$\ln\left(\frac{N(V)}{N_{tot}}\right) = \ln\tilde{\lambda} - \lambda V$$

i.e. $\ln\left(N(V)/N_{tot}\right)$ should be a linear function of V with the slope $-\lambda$. The value of λ can be found from linear least-square fitting.

In Figs. 6.6 (a), (c) we plot average concentration $N(V)$ and probability $N(V)/N_{tot}$ as functions of V. Plots (b) and (d) on the right hand side of 6.6 show logarithms of average concentration and probability as functions of V. From the graph of the average concentration or probability we can see that the solution starts decaying only after $V \geq 35$. Therefore, in the least square fitting we use only values of $N(V)/N_{tot}$ for $V \geq 35$. The fitted straight lines are shown in Fig. 6.6 (d) and their slopes at times $t = 0.125$, 0.25 are $-\lambda_{0125} = -0.01436$ and $-\lambda_{025} = -0.0072972$, re-

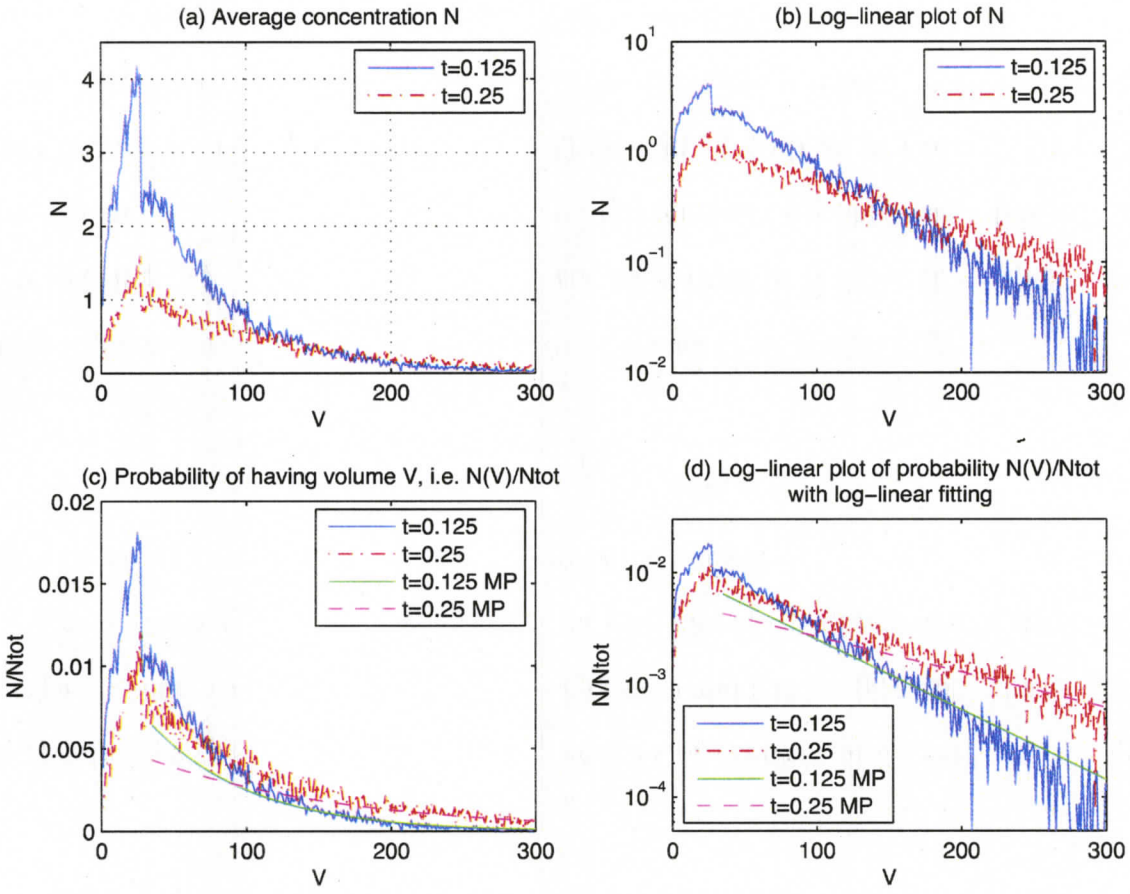

Figure 6.6: Average concentration $N(V)$ obtained from initial uniform distribution at $t = 0.125$ and $t = 0.25$.

spectively. The corresponding values of $\tilde{\lambda}$ are $\tilde{\lambda}_{0125} = 0.010665$ and $\tilde{\lambda}_{025} = 0.0055892$. Therefore, using (6.5) the relative frequency or probability at times $t = 0.125$, 0.25 can be approximated by

$$\left.\frac{N(V)}{N_{tot}}\right|_{t=0.125} = 0.010665 \cdot \exp(-0.01436 \cdot V) \tag{6.6}$$

and

$$\left.\frac{N(V)}{N_{tot}}\right|_{t=0.25} = 0.0055892 \cdot \exp(-0.0072972 \cdot V) \tag{6.7}$$

Note that as time doubles from $t = 0.125$ to $t = 0.25$, the values of both λ and $\tilde{\lambda}$ decrease approximately by half, which suggests that these parameters decrease linearly with $1/t$. This is indeed the case and we will justify it later.

We can also compare how close parameters λ and $\tilde{\lambda}$ are. As time $t = 0.125$, the difference between these parameters is $|\lambda - \tilde{\lambda}| = 0.0036943$ whereas at $t = 0.25$, the difference decreases to the value 0.0017079, which is about half of the difference at $t = 0.125$. As we will see later, the difference $|\lambda - \tilde{\lambda}|$ also decays linearly with $1/t$ at least up to time $t = 1$.

From graphs of the probability $N(V)/N_{tot}$ on Fig. 6.6 (c) at times $t = 0.125$ and $t = 0.25$ as well as their fitted negative exponential function approximations (6.6) and (6.7) one can observe that the agreement is better for large volumes V and the fitted value underestimate the exponential decay rate for moderate values of V. For example, at $t = 0.125$, the agreement is achieved for $V > 120$ whereas at $t = 0.25$ functions agree only for $V > 180$.

As time evolves, the number of droplets in a cloud decreases due to coalescence. This process can be observed in Fig. 6.7 (a) where we see that the average concentration $N(V)$ at each later time is below the average concentration obtained at the previous time at least for those volumes V at which concentration is not very close to zero. The number of droplets decreases with size, therefore for very large volumes V, curves representing $N(V)$ intersect each other due to fluctuations when values of $N(V)$ are close to zero. We can also do linear least square fitting (see Fig. 6.7 (d)) to

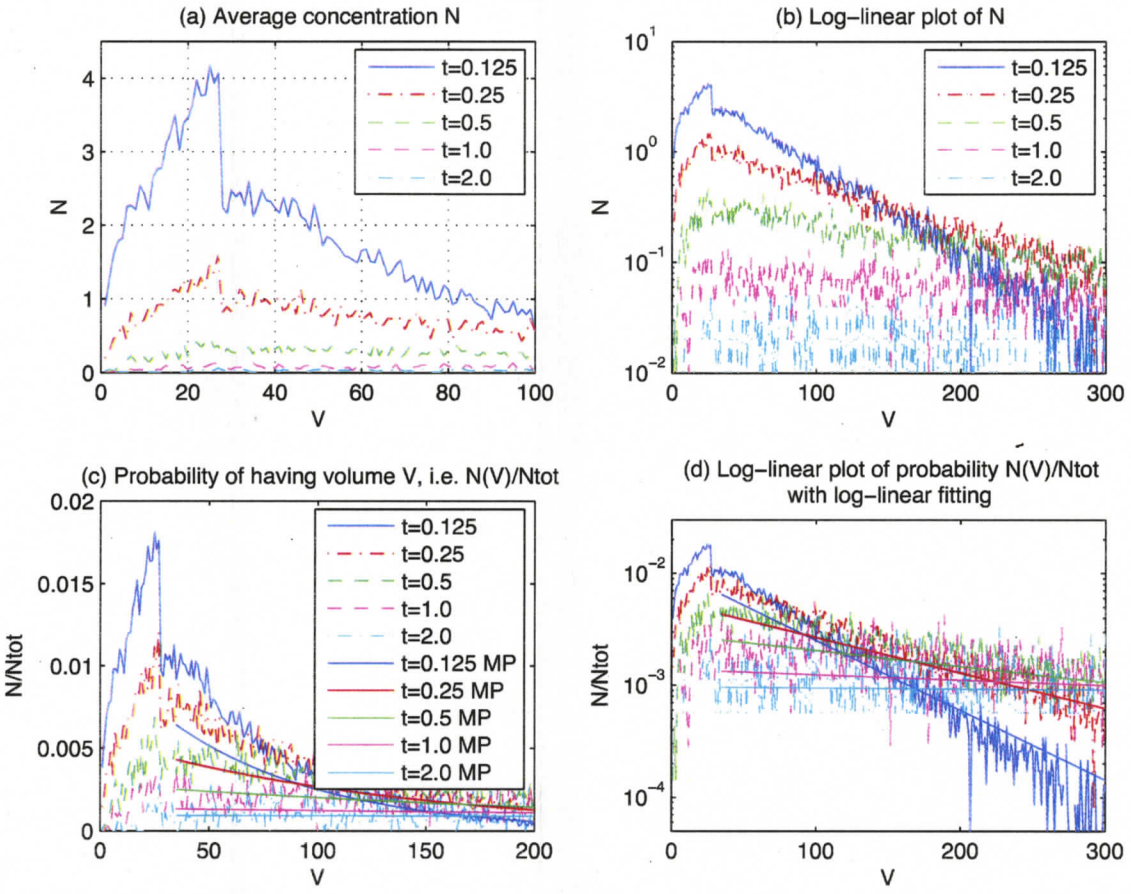

Figure 6.7: Average concentration $N(V)$ obtained from initial uniform distribution at the sequence of times $t = 0.125$, 0.25, 0.5, 1.0 and 2.0.

find rates $-\lambda$ of exponential decay at each time 0.5, 1.0 and 2.0 and compare them with previously found values. In Fig. 6.8 (a) we plot λ and $\tilde{\lambda}$ as functions of t. Fig. 6.8 (b) contains the plot of the difference $|\lambda - \tilde{\lambda}|$ as a function of time.

As was noted earlier, as time doubles, values of λ, $\tilde{\lambda}$ and $|\lambda - \tilde{\lambda}|$ decrease approximately by half. In case of the difference $|\lambda - \tilde{\lambda}|$, this is true only up to time $t = 1$ after which the difference increases a little bit. We can convince ourselves that these

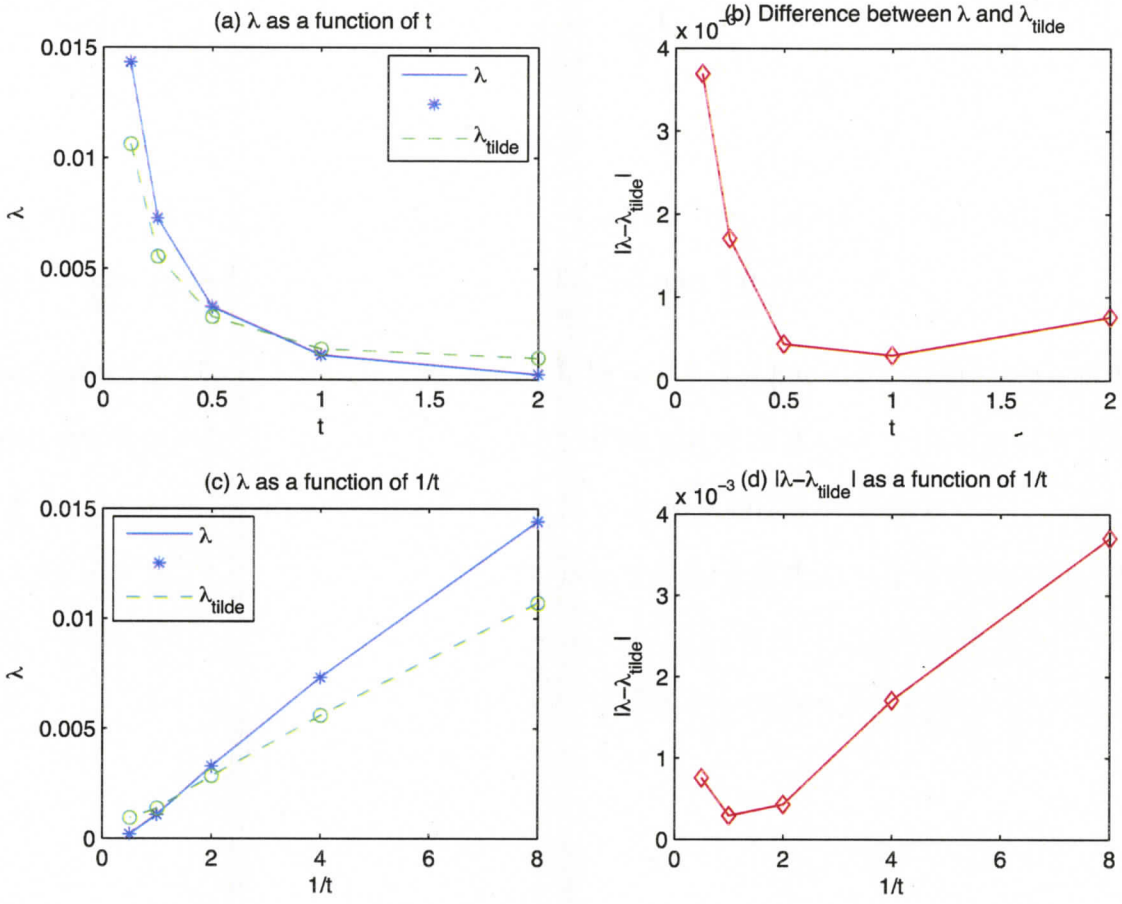

Figure 6.8: Evolution of λ, $\tilde{\lambda}$ and $|\lambda - \tilde{\lambda}|$ with time t.

parameters decay linearly in $1/t$ if we plot λ, $\tilde{\lambda}$ and $|\lambda - \tilde{\lambda}|$ as functions of $1/t$. Fig. 6.8 (c) and (d) show that these graphs indeed look similar to straight lines except for the difference $|\lambda - \tilde{\lambda}|$, for which the straight line behavior is only observed up to approximately time $t = 1$. If we assume that λ, $\tilde{\lambda}$ and $|\lambda - \tilde{\lambda}|$ can be approximated by Ct^{-p}, then logarithm of this expression is a linear function of $\ln t$ and the linear least squares method can be used to find values of C and p. Indeed, we find that

$$\lambda = 0.00086511 \cdot t^{-1.4824}, \quad \tilde{\lambda} = 0.0016033 \cdot t^{-0.89067}$$

and

$$|\lambda - \tilde{\lambda}| = 0.00024723 \cdot t^{-1.2921}$$

As we can see, each of these parameters decays approximately as $1/t$. We should also note that the agreement between the relative frequency $N(V)/N_{tot}$ with the fitted exponentially decaying function is achieved for large droplet sized. For earlier times, functions agree starting from smaller value of droplet volume V.

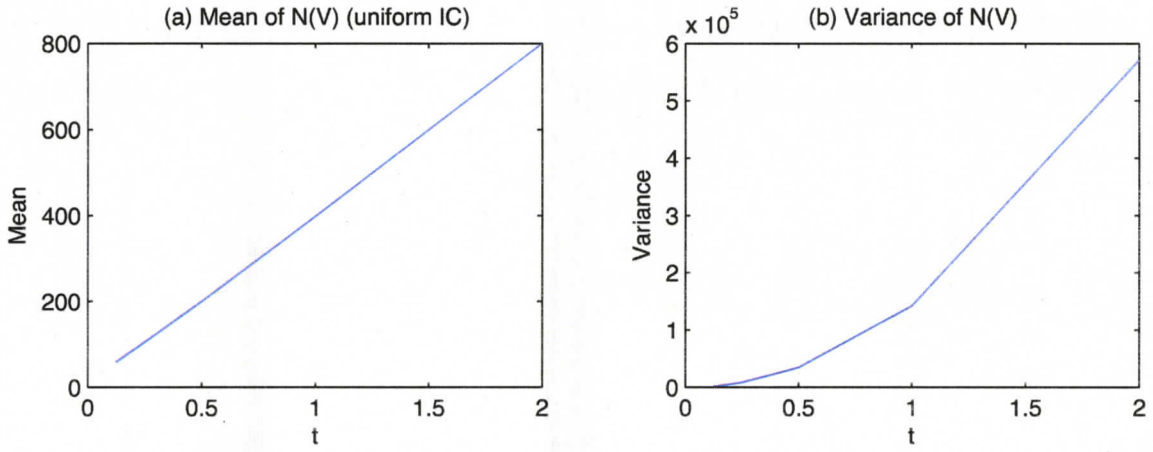

Figure 6.9: (a) Mean; (b) Variance of the average concentration $N(V)$ as a function of V at times $t = 0.125$, 0.25, 0.5, 1.0 and 2.0 obtained from initially uniform distribution.

Recall that the average concentration $N(V)$ is the expected value that there are N droplets of volume V. We can find the mean and the variance of this distribution of droplets with volume. Then the mean is

$$E(N(V)) = \mu = \sum_{i=0}^{\infty} V_i \cdot Prob\{\text{on average there are } N(V_i) \text{ droplets of volume } V_i\}$$

or

$$\mu = \sum_{i=0}^{\infty} V_i \cdot \frac{N(V_i)}{N_{tot}}$$

During computations we operate with finite number of volumes, therefore

$$\mu = \sum_{i=0}^{V_{max}} V_i \cdot \frac{N(V_i)}{N_{tot}}.$$

Due to the process of coalescence, larger droplets are being formed and, hence, V_{max} increases with time. Probabilities do not exceed value of 1 and, as a consequence, the mean of $N(V)$ increases as time increases. We can see this in Fig. 6.9 (a) where the mean of $N(V)$ is plotted as a function of time t. The values of μ at times 0.125, 0.25, 0.5, 1.0 and 2.0 are 60.6387, 106.9645, 201.2205, 397.7491, 798.4026, respectively. We also see that as time doubles, the value of the means also doubles. Hence, the mean grows linearly with time. We can also see this on the graph in Fig. 6.9 (a). Similarly, we can analyze the variance of $N(V)$ as a function of V. Recall that the variance equals the difference of the second moment and the square of the expected value and the second moment is

$$E(N^2) = \sum_{i=0}^{V_{max}} V_i^2 \cdot \frac{N(V_i)}{N_{tot}}$$

and

$$Var(N) = E(N^2) - [E(N)]^2 = E(N^2) - \mu^2.$$

Fig. 6.9 (b) contains the plot of the variance $Var(V)$ and it also grows with time. The variance grows faster then the mean. In fact, its values are $10^5 * 0.0300$, $10^5 * 0.0996$, $10^5 * 0.3589$, $10^5 * 1.4304$ and $10^5 * 5.6997$. The growth rate is approximately 3/2 (i.e variance is proportional to $t^{3/2}$) since as time doubles, the value of the variance increases by 3 times. It would be linear if the value of variance also doubled or quadratic if the variance increases by a factor of 4. The reason why both mean and variance grow with time is that droplets grow with time while their number decreases, hence particles with smaller volume have less input on the mean and variance. Again, this is the feature of direct stochastic simulations and can be overcome by applying some particle combining techniques mentioned above.

In conclusion, we have established that the distribution in volumes can be approximated by the negative exponential $\tilde{\lambda} \cdot \exp(-\lambda V)$ and $\tilde{\lambda}$ tends to λ as time increases.

Similar analysis can be conducted for the average concentration $N(V)$ obtained from initial Poisson distribution. Results are similar to the case of initial uniform distribution although there are some differences.

Analyzing Fig. 6.10 one can observe that at time $t = 0.125$, the maximum value of the average concentration $N(V)$ obtained from Poisson distribution is about 7.8 and this is twice greater than the maximum from the uniform initial condition. At next time $t = 0.25$, the maximum of both solutions is about 2. Therefore, maximum in both cases decreased approximately by half as time doubled. The maximum concentration using uniform initial condition occurs at $V = 30$ whereas in the Poisson distribution case, the maximum is achieved at $V = 10$. Therefore, the linear least square fitting for the Poisson case can be done for volumes $V \geq 10$, not 30 or 35 as in the uniform

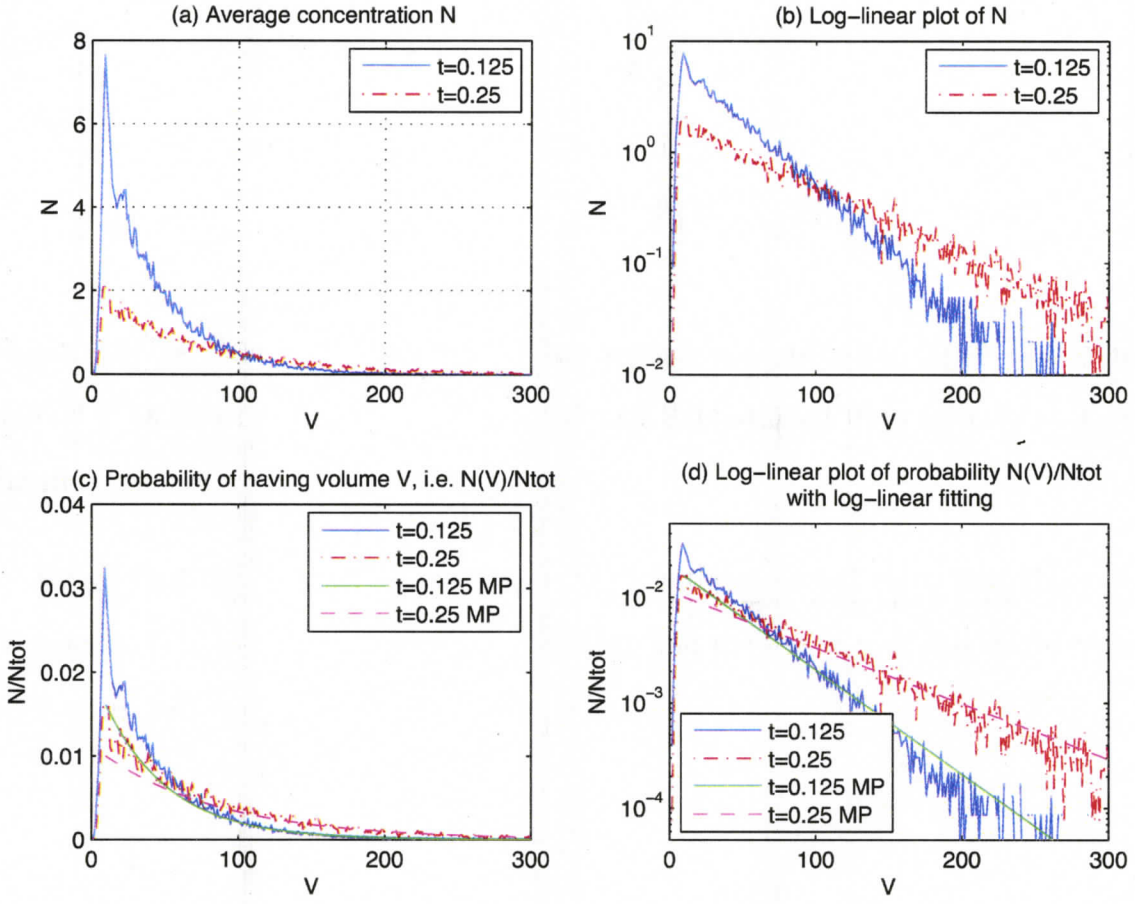

Figure 6.10: Average concentration $N(V)$ obtained from initial Poisson distribution at $t = 0.125$ and $t = 0.25$.

case.

Agreement between probability and the fitted exponential distribution function at $t = 0.125$ is achieved for $V \geq 70$ and at $t = 0.25$ for $V \geq 100$. Recall that in the uniform case, the agreement was achieved for $V \geq 120$ and $V \geq 180$, respectively. Therefore, in the Poisson case, probability and fitted exponential function start agreeing at about twice smaller droplet volumes.

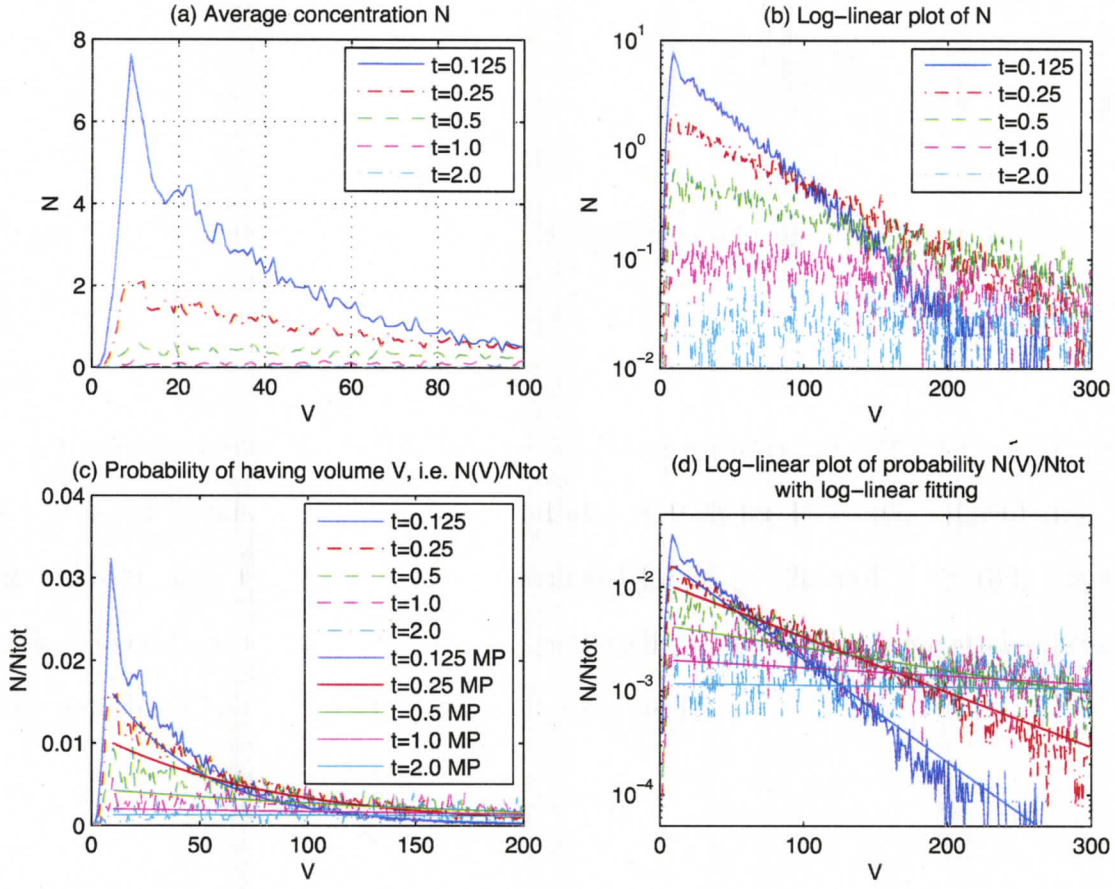

Figure 6.11: Average concentration $N(V)$ obtained from initial Poisson distribution at the sequence of times $t = 0.125$, 0.25, 0.5, 1.0 and 2.0.

Studying plots in Fig. 6.11 at the sequence of times from $t = 0.125$ to $t = 2$, we see that average concentration decays faster than in the uniform case. The same conclusion can be made looking at the graphs of the parameter λ in Fig. 6.12 since $-\lambda$ stands for the exponential decay of the relative frequency $N(V)/N_{tot}$. The value of λ at $t = 0.125$ is 0.0229 using Poisson initial condition and this is about twice bigger than corresponding value 0.01436 for the uniform distribution. Nevertheless, plots in

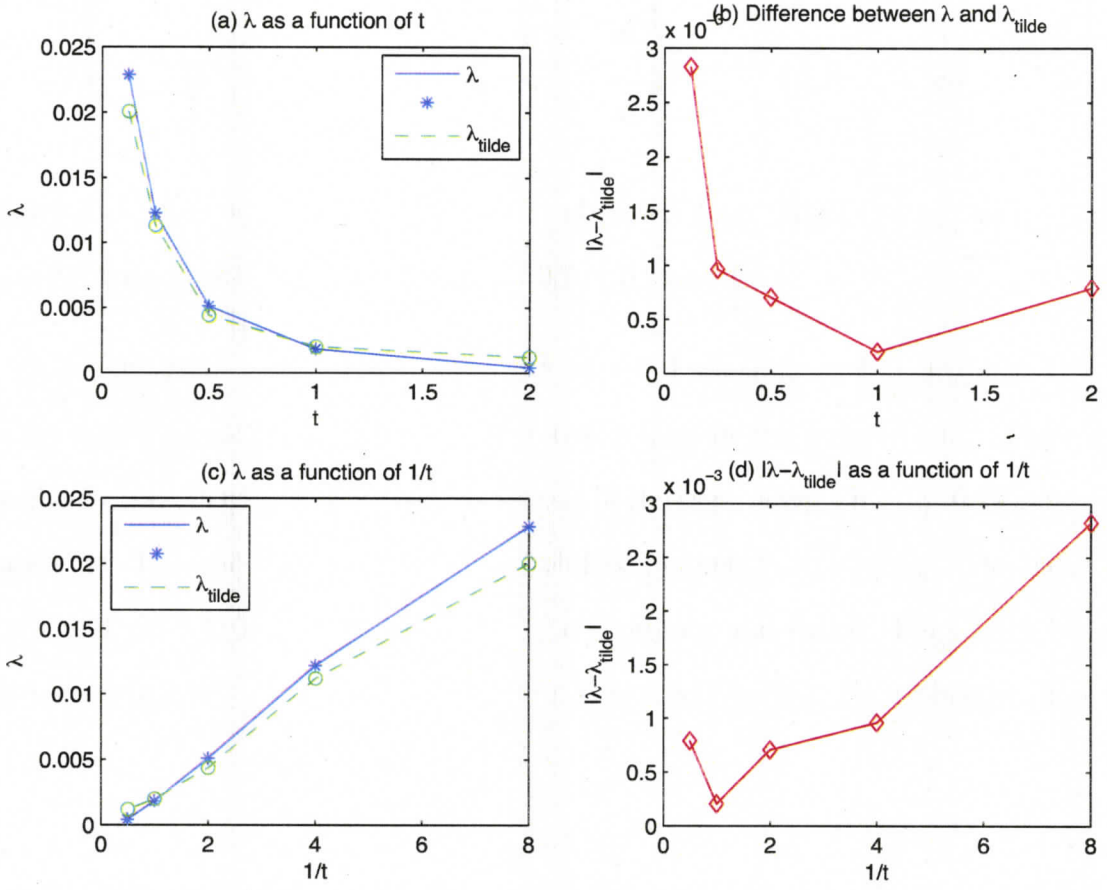

Figure 6.12: Evolution of λ, $\tilde{\lambda}$ and $|\lambda - \tilde{\lambda}|$ with time t.

Fig. 6.12 (c) and (d) indicate that parameters λ, $\tilde{\lambda}$ and their difference $|\lambda - \tilde{\lambda}|$ decay approximately linearly in $1/t$ for until time $t = 2$ at least for the first two parameters and until $t = 1$ for their difference.

We can study the mean and the variance of $N(V)$ as in the case of initially uniform distribution. When initial distribution is Poissonian, the mean also increases linearly with time, while the variance grows quadratically, even faster than in the uniform distribution case as we observe from Fig. 6.13.

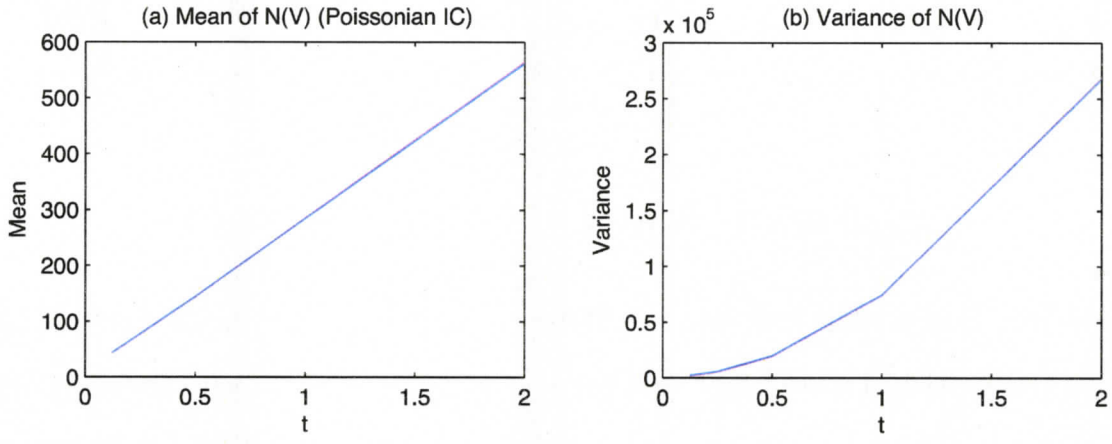

Figure 6.13: (a) Mean; (b) Variance of the average concentration $N(V)$ as a function of V at times $t = 0.125$, 0.25, 0.5, 1.0 and 2.0 obtained from initially Poissonian distribution.

The next Fig. 6.14 we analyze the total number of droplets in a cloud and we see that it decreases dramatically with time.

We can also check that the total mass is also conserved as in the case of the initial uniform condition.

Next we analyze whether the average concentration N can be approximated with Marshall-Palmer distribution in terms on large radii/diameters and not volumes as in our case. As Fig. 6.15 shows, this is not the case. Indeed, if N had exponential decay as a function of, say, radius r, i.e. $N(r) = \lambda \exp(-\lambda r)$, then the logarithm of $N(r)$ would be a linear function of r. From Fig. 6.15 (b) where we plot $\ln N(r)$ as a function of r, we do not get a linear function. It is rather at least quadratic, which indicates that concentration N has more complicated behavior than the exponential function of r. From the other point, we established that N has exponential decay

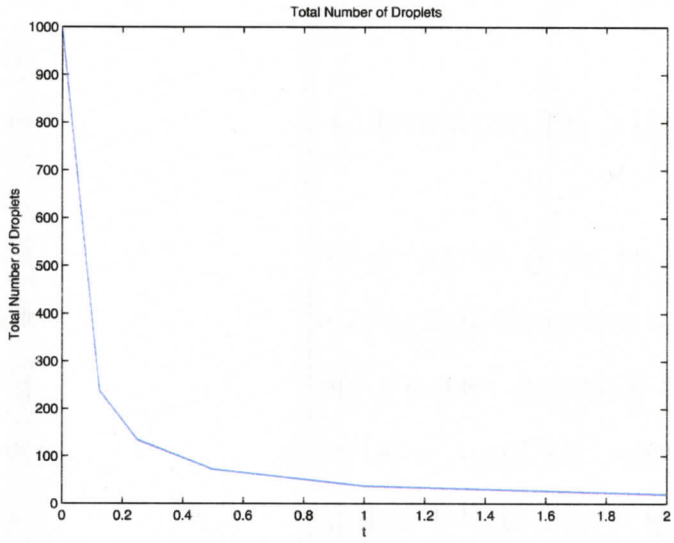

Figure 6.14: Total Number of Droplets in a Cloud

as a function of volumes V and volume depends on radius r nonlinearly $V = \frac{4\pi}{3}r^3$. Therefore, we should not anticipate exponential decay of N as a function of r and graphs in Fig. 6.15 support this.

We can conclude by saying that the relative frequency $N(V)/N_{tot}$ obtained either from uniform or Poisson initial distribution of droplets can be approximated by Marshall-Palmer distribution function that is negative exponential function

$$f(V) = \lambda \cdot \exp(-\lambda V).$$

At each considered time we are able to write

$$\frac{N(V)}{N_{tot}} \approx \tilde{\lambda} \cdot \exp(-\lambda V) \tag{6.8}$$

and $\tilde{\lambda}$ approaches λ as time increases. Functions on the left and right hand sides of equation (6.8) agree starting from some threshold volume V_{min} and this minimum

volume increases as time increases. As demonstrated numerically the rate of exponential decay is about twice bigger for the case of Poisson distribution but in both cases, the rates decay linearly in $1/t$.

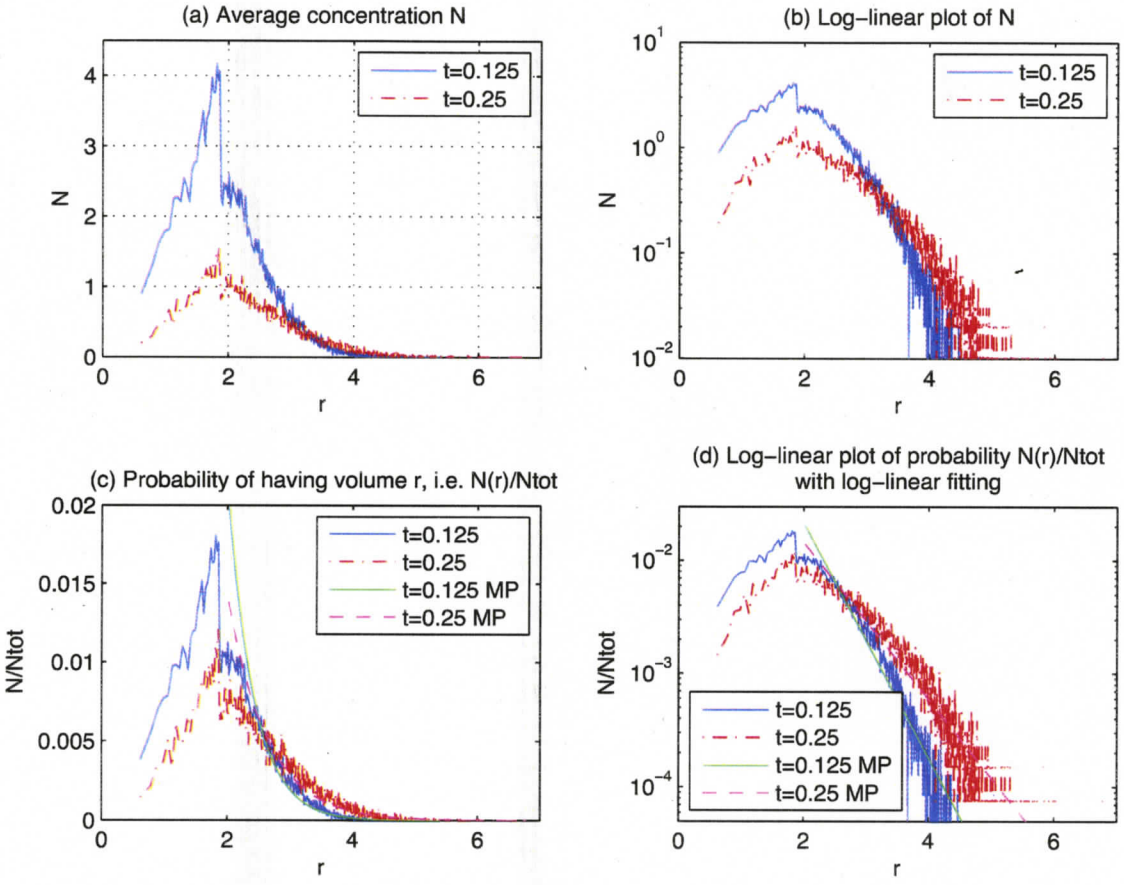

Figure 6.15: (a) average concentration $N(r)$ as a function of radius r obtained from initial uniform distribution at $t = 0.125$ and $t = 0.25$; (b) log-linear plot of $N(r)$; (c) probability of having radius r; (d) log-linear plot of probability of having radius r with linear fitting

Chapter 7

Conclusions

1. The process of particle growth in a warm cloud caused by the process of coalescence is studied using stochastic and kinetic models.

2. The stochastic coalescence process introduced by Gillespie [J. Atmos. Sci. 29 (1972) 1496–1510] is implemented numerically with Monte Carlo algorithm developed by Gillespie [J. Atmos. Sci. 32 (1975) 1977–1989].

3. It is demonstrated that the outcome of the kinetic model matches well the true stochastic averages even if the number concentration of particles involved is small for well mixed suspensions.

4. In the case of one large particle settling through a monodisperse suspension of small particles, which is an example of a poorly mixed suspension, it is shown that the solution to the stochastic equation predicts about twice the growth rate of the average large particle than the kinetic model.

5. It is demonstrated that the normalized average concentration for large volumes

obtained from the initial uniform and Poisson distributions in the stochastic coalescence model can be approximated by the Marshall-Palmer-like distribution law as a function of volume V and not as a function of r as originally introduced by Marshall-Palmer.

Bibliography

[1] Aldous, D. J. Deterministic and stochastic models for coalescence (aggrégation and coagulation): a review of the mean-field theory for probabilists. *Bernoulli 5*, 1 (1999), 3–48.

[2] Angeli, P., and Hewitt, G. Drop size distributions in horizontal oil-water dispersed flows. *Chemical Engineering Science 55*, 2000 (16), 3133–3143.

[3] Baker, M. Cloud microphysics and climate. *Science 276* (1997), 1072–1078.

[4] Bayewitz, M., J., Y., Katz, S., and Shinnar, R. Extent of correlations in a stochastic coalescence process. *Journal of the Atmospheric Sciences 31*, 6 (1974), 1604–1614.

[5] Beard, K., and Ochs, H. Warm-rain initiation - an overview of microphysical mechanisms. *Journal of Applied Meteorology 32*, 4 (1993), 608–625.

[6] Berry, E., and R.L., R. Analysis of cloud drop growth by collection .1. Double distributions. *Journal Of The Atmospheric Sciences 31*, 7 (1974), 1814–1824.

[7] BERRY, E., AND R.L., R. Analysis of cloud drop growth by collection .2. Single initial distributions. *Journal Of The Atmospheric Sciences 31*, 7 (1974), 1825–1831.

[8] BERRY, E. Cloud droplet growth by collection. *Journal Of The Atmospheric Sciences 24*, 6 (1967), 688–701.

[9] BLECK, R. A fast, approximative method for integrating stochastic coalescence equation. *Journal Of Geophysical Research 75*, 27 (1970), 5165–&.

[10] BRADIE, B. *A Friendly Introduction to Numerical Analysis.* Prentice Hall, 2006.

[11] BRAHAM, R. What is the role of ice in summer rain-showers. *Journal Of The Atmospheric Sciences 21*, 6 (1964), 640–645.

[12] BYERS, H., AND HALL, R. A census of cumulus-cloud height versus precipitation in the vicinity of Puerto-Rico during the winter and spring of 1953-1954. *Journal of Meteorology 12*, 2 (1955), 176–178.

[13] DIEMER, R., AND OLSON, J. A moment methodology for coagulation and breakage problems: Part 2 - moment models and distribution reconstruction. *Chemical Engineering Science 57*, 12 (2002), 2211–2228.

[14] DIEMER, R., AND OLSON, J. A moment methodology for coagulation and breakage problems: Part 1 - analytical solution of the steady-state population balance. *Chemical Engineering Science 2002*, 12 (57), 2193–2209.

[15] DRAKE, R. Scalar transport-equation of coalescence theory - moments and kernels. *Journal Of The Atmospheric Sciences 29*, 3 (1972), 537–547.

[16] Eibeck, A., and Wagner, W. Approximative solution of the coagulation-fragmentation equation by stochastic particle systems. *Stochastic Anal. Appl. 18*, 6 (2000), 921–948.

[17] Eibeck, A., and Wagner, W. An efficient stochastic algorithm for studying coagulation dynamics and gelation phenomena. *SIAM J. Sci. Comput. 22*, 3 (2000), 802–821 (electronic).

[18] Eibeck, A., and Wagner, W. Stochastic algorithms for studying coagũlation dynamics and gelation phenomena. *Monte Carlo Methods Appl. 7*, 1-2 (2001), 157–165. Monte Carlo and probabilistic methods for partial differential equations (Monte Carlo, 2000).

[19] Eyre, D., Wright, C., and Reuter, G. Spline-collocation with adaptive mesh grading for solving the stochastic collection equation. *Journal Of Computational Physics 78*, 2 (1988), 288–304.

[20] Frenklach, M., and Harris, S. Aerosol dynamics modeling using the method of moments. *Journal Of Colloid And Interface Science 118*, 1 (1987), 252–261.

[21] Frenklach, M. Dynamics of discrete distribution for Smoluchowski coagulation model. *Journal Of Colloid And Interface Science 108*, 1 (1985), 237–242.

[22] Gelbard, F., and Seinfeld, J. H. Numerical solution of the dynamic equation for particulate systems. *J. Comput. Phys. 28*, 3 (1978), 357–375.

[23] GILLESPIE, D. Stochastic coalescence model for cloud droplet growth. *Journal Of The Atmospheric Sciences 29*, 8 (1972), 1496–1510.

[24] GILLESPIE, D. Exact method for numerically simulating stochastic coalescence process in a cloud. *Journal Of The Atmospheric Sciences 32*, 10 (1975), 1977–1989.

[25] GOLOVIN, A. The solution of the coagulation equation for cloud droplets in a rising air current. *Izvestiya Akademii Nauk SSSR Seria Geofizika 5* (1963), 783–&.

[26] GOODSON, M., AND KRAFT, M. Simulation of coalescence and breakage: An assessment of two stochastic methods suitable for simulating liquid-liquid extraction. *Chemical Engineering Science 59*, 18 (2004), 3865–3881.

[27] GROSSCHMIDT, D., BOCKHORN, H., GOODSON, M., AND KRAFT, M. Two approaches to the simulation of silica particle synthesis. *Proceedings Of The Combustion Institute 29*, 1 (2003), 1039–1046.

[28] HEYWOOD, G. Rain formation in the tropics. *Quarterly Journal of the Royal Meteorological Society 66* (1940), 46.

[29] HIDY, G., AND BROCK, J. *The Dynamics of Aerocolloidal Systems.* Pergamon, Oxford, 1970.

[30] HOUNSLOW, M., RYALL, R., AND MARSHALL, V. A discretized population balance for nucleation, growth, and aggregation. *A.I.Ch.E. Journal 34*, 11 (1988), 1821–1832.

[31] Physics of cloud, Cited: August 11, 2006.

[32] JONAS, P. Turbulence and cloud microphysics. *Atmospheric Research 40*, 2-4 (1996), 283–306.

[33] KUMAR, S., AND RAMKRISHNA, D. On the solution of population balance equations by discretization .1. A fixed pivot technique. *Chemical Engineering Science 51*, 8 (1996), 1311–1332.

[34] KUMAR, S., AND RAMKRISHNA, D. On the solution of population balance equations by discretization .2. a moving pivot technique. *Chemical Engineering Science 51*, 8 (1996), 1333–1342.

[35] LAGE, P. Comments on the "An analytical solution to the population balance equation with coalescence and breakage - the special case with constant number of particles" by D.P. Patil and J.R.G. Andrews [Chemical Engineering Science 53(3) 599-601]. *Chemical Engineering Science 57*, 19 (2002), 4253–4254.

[36] LAURENZI, I., AND DIAMOND, S. Kinetics of random aggregation-fragmentation processes with multiple components. *Physical Review E 67*, 5 (2003), Art. No. 051103.

[37] LEE, K., AND MATSOUKAS, T. Simultaneous coagulation and break-up using constant-N Monte Carlo. *Powder Technology 110*, 1-2 (2000), 82–89.

[38] LIN, Y., LEE, K., AND MATSOUKAS, T. Solution of the population balance equation using constant-number Monte Carlo. *Chemical Engineering Science 57*, 12 (2002), 2241–2252.

[39] LITSTER, J., SMIT, D., AND HOUNSLOW, M. Adjustable discretized population balance for growth and aggregation. *A.I.Ch.E. Journal 41*, 3 (1995), 591–603.

[40] LIU, Y., AND CAMERON, I. A new wavelet-based method for the solution of the population balance equation. *Chemical Engineering Science 56*, 18 (2001), 5283–5294.

[41] LUSHNIKOV, A. Coagulation in finite systems. *Journal Of Colloid And Interface Science 65*, 2 (1978), 276–285.

[42] MARSHALL, J., AND PALMER, W. The distribution of raindrops with size. *Journal Of Meteorology 5*, 4 (1948), 165–166.

[43] MCCOY, B., AND MADRAS, G. Analytical solution for a population balance equation with aggregation and fragmentation. *Chemical Engineering Science 58*, 13 (2003), 3049–3051.

[44] MORDY, W., AND EBER, L. Observations of rainfall from warm clouds. *Quarterly Journal Of The Royal Meteorological Society 80*, 343 (1954), 48–&.

[45] NICMANIS, M., AND HOUNSLOW, M. Finite-element methods for steady-state population balance equations. *A.I.Ch.E. Journal 44*, 10 (1998), 2258–2272.

[46] PATIL, D., AND ANDREWS, J. An analytical solution to continuous population balance model describing floc coalescence and breakage - a special case. *Chemical Engineering Science 53*, 3 (1998), 599–601.

[47] Pinsky, M., and Khain, A. Turbulence effects on droplet growth and size distribution in clouds - a review. *Journal Of Aerosol Science 28*, 7 (1997), 1177–1214.

[48] Ramkrishna, D. Analysis of population balance. 4. the precise connection between Monte-Carlo simulation and population balances. *Chemical Engineering Science 36*, 7 (1981), 1203–1209.

[49] Ross, S. *Introduction to Probability Models.* Academic Press, Inc., 1989.

[50] Sabelfeld, K. K., Rogasinsky, S. V., Kolodko, A. A., and Levykin, A. I. Stochastic algorithms for solving Smolouchovsky coagulation equation and applications to aerosol growth simulation. *Monte Carlo Methods Appl. 2*, 1 (1996), 41–87.

[51] Scott, W. Poisson statistics in distributions of coalescing droplets. *Journal Of The Atmospheric Sciences 24*, 2 (1967), 221–225.

[52] Scott, W. On connection between telford and kinetic-equation approaches to droplet coalescence theory. *Journal Of The Atmospheric Sciences 25*, 5 (1968), 871– 873.

[53] Seesselberg, M., Trautmann, T., and Thorn, M. Stochastic simulations as a benchmark for mathematical methods solving the coalescence equation. *Atmospheric Research 40*, 1 (1996), 33–48.

[54] Seigneur, C., Hudischewskyj, A., Seinfeld, J., Whitby, K., Whitby, E., Brock, J., and Barnes, H. Simulation of aerosol dynamics - a com-

parative review of mathematical-models. *Aerosol Science And Technology 5*, 2 (1986), 205–222.

[55] Smith, M., and Matsoukas, T. Constant-number Monte Carlo simulation of population balances. *Chemical Engineering Science 53*, 9 (1998), 1777–1786.

[56] Squires, P. Project shower - investigation on warm rain in the hawaiian islands. *Nature 175*, 4461 (1955), 748–750.

[57] Telford, J., Thorndike, N., and Bowen, E. The coalescence between small water drops. *Quarterly Journal Of The Royal Meteorological Society 81*, 348 (1955), 241–250.

[58] Telford, J. Clouds with turbulence; the role of entrainment. *Atmospheric Research 40*, 2-4 (1996), 261–282.

[59] Tzivion, S., Feingold, G., and Levin, Z. (Tzivion, S.T.=Tzitzvashvili, S.T.) An efficient numerical-solution to the stochastic collection equation. *Journal Of The Atmospheric Sciences 44*, 21 (1987), 3139–3149.

[60] Valioulis, I., and List, E. A numerical evaluation of the stochastic completeness of the kinetic coagulation equation. *Journal Of The Atmospheric Sciences 41*, 16 (1984), 2516–2529.

[61] Valioulis, I. Coagulation in the aquatic environment - theory and practice. *Advances In Colloid And Interface Science 24*, 2-3 (1986), 81–102.

[62] Vanni, M. Approximate population balance equations for aggregation-breakage processes. *Journal Of Colloid And Interface Science 221*, 2 (2000), 143–160.

[63] VON SMOLUCHOWSKI, M. Three presentations on diffusion, molecular movement according to brown and coagulation of colloid particles. *Physikalische Zeitschrift 17* (1916), 557–571.

[64] WILLIAMS, M., AND LOYALKA, S. *Aerosol Science, Theory and Practice.* Pergamon, New York, 1991.